

We are IntechOpen, the world's leading publisher of Open Access books Built by scientists, for scientists

6,900

Open access books available

185,000

International authors and editors

200M

Downloads

Our authors are among the

154

Countries delivered to

TOP 1%

most cited scientists

12.2%

Contributors from top 500 universities



WEB OF SCIENCE™

Selection of our books indexed in the Book Citation Index
in Web of Science™ Core Collection (BKCI)

Interested in publishing with us?
Contact book.department@intechopen.com

Numbers displayed above are based on latest data collected.
For more information visit www.intechopen.com



Effects of Automatic Flight Control System on Chinook Underslung Load Failures

Marilena D. Pavel

*Faculty of Aerospace Engineering, Delft University of Technology
The Netherlands*

1. Introduction

One of the major helicopter attributes is its ability to transport cargo externally in the form of external slung loads (see Fig. 1). Commercial and military operators accept the fact that using a helicopter for external load transportation is usually expensive in terms of both money and time. However, helicopters still have the significant advantage of accessing unreachable sites. Operations of helicopters with external loads impose limitations to the use of the helicopter, as for example: helicopter maximum forward speed is usually severely reduced because of the danger on dynamic instabilities of the load; due to external load the aerodynamic drag can become excessive, resulting in power and control limitations on the helicopter. The problem addressed in this chapter concerns the behaviour of a helicopter following the premature breakdown of one of its cables sustaining the slung load. As a specific example, the Chinook helicopter CH-47B with an external load will be considered. The CH-47 (Chinook) is a twin-engine tandem rotor helicopter (see Fig. 1) designed for all-weather, medium-sized transport type operations. The three bladed rotors are driven in opposite directions (front rotor rotates anticlockwise, rear rotor rotates clockwise) through interconnecting shafts which enable both rotors to be driven by either engine. The rotor heads are fully articulated, with pitch, flapping, and lead-lag hinges.



Fig. 1. Chinook helicopter transporting single and multiple loads (Courtesy of the Royal Netherlands Air Force)

The goal of the chapter will be to implement the advanced automatic flight control system AFCS of the Chinook CH-47 (analogue in Chinook D-version and digital in the latest version F) into a generic Chinook model developed at Delft University of Technology (Van der Kamp et. Al (2005), Reijm, Pavel&Bart (2006), Pavel(2007), Pavel(2010)) and investigate the effects that AFCS may have on the recovery prospects of the Chinook helicopter after a failure scenario of its load. In other words, this chapter proposes to analyse how the advanced AFCS, implemented in general in order to improve the handling qualities characteristics, may improve/degrade the CH-47 behaviour during emergency situations such as failure scenarios of its suspended load(s). Searching in the specialist literature for research on this particular area of load failures and the AFCS effects on assisting/hindering the pilot during load failure recovering revealed that the subject has not been really investigated. A few publications have been identified dealing with load failure scenarios - they address mainly a rather different problem, i.e. the situation in which a load is moving within an aircraft before being dropped - and none considers the effects that AFCS may have on helicopter behaviour during such emergency situations. Some relevant publications for understanding the problems related to the dynamics of a helicopter with a slung load are given below.

(Lucasen and Sterk, 1965) developed a first theoretical study of the dynamics of a single rotor helicopter carrying a slung load in hovering flight using a 3-dof longitudinal helicopter model including translation and attitude of the helicopter and load displacement w.r.t. the helicopter. They demonstrated that the phugoid stability depended on the cable length, decreasing with increasing cable length. (Dukes, 1973a) studied the stability characteristics of a single rotor helicopter with slung load near hover showing that with large pitch damping, the translational motion is only weakly coupled to the attitude and load motions. In a second study (Dukes, 1973b) concentrated on the stability of the load during different manoeuvres (acceleration-deceleration, changing the hover location and arresting a pendulous load motion) identifying some fundamental features of load control which can be utilized as basis for an open loop control strategy. (Feaster, Poli & Kirchhoff, 1977) studied the stability in forward flight of a single-rotor helicopter carrying a container, showing that long cables, high speeds and low weights increased the stability of the loads. Their results were contradicted by (Cliff&Bailey,1975) who obtained that longer cables were destabilizing, this probably due to different load aerodynamics considered. Both last papers underlined the importance of the load aerodynamics in studying the stability of helicopter-slung load systems, where dynamic instabilities can be triggered by unsteady load aerodynamics. The most dominant form of load aerodynamic instability is a yawing divergence that couples with the load lateral modes. (Gabel, 1968) studied the slung load “vertical bounce” phenomenon, i.e. a resonant condition inherent to elastic sling load systems that occurs when the natural frequency of the sling load is close to one of the rotor frequencies. This mode can be exacerbated by the pilot’s inertial reaction to vertical accelerations, leading to a vertical force being transmitted to the collective stick. To account for vertical bounce phenomenon one has to consider elastic suspensions. The author proposed several solutions to the pilot induced vertical bounce problem, the most promising being a low gain boost system which was meant to produce very low output for small pilot inputs and normal output for normal pilot inputs. For forwards speeds above 40 knots, the author showed that the effects of rotor downwash on the load aerodynamics are not important. (Nagabhushan, 1985) developed a non-linear body-flap model of a single rotor-helicopter and studied the stability characteristics of the helicopter-slung load system. He

found that operating with a long sling cable damps out the sling-load pendulum mode lateral oscillation and the helicopter longitudinal phugoid; however, the associated sling-load pitch oscillation and the helicopter Dutch roll mode become unstable. Suspending the sling load from a point ahead of the helicopter centre of gravity was found to stabilize the helicopter lateral oscillation; suspending it from a point aft of the centre of gravity caused instability. (Sheldon, 1978) concluded from experiments that a large number of instabilities are initiated by load yawing motions. A relatively easy way of obtaining an increased yaw resistance is to use a multipoint suspension system rather than a single point suspension. His experiments have shown that an inverted 'V' suspension system provides significant yaw resistance, while also minimizing the load trail angle. (Prabhakar, 1978) developed a non-linear single rotor helicopter-slung load model in multipoint suspension showing that the number, spacing and placement of the suspension points and the topology of the suspension cables are all important. The load is capable of changing almost completely the helicopter rigid body modes, generally destabilizing. Also, there exists significant coupling between the load and the helicopter lateral modes. The helicopter longitudinal modes on the other hand are affected little by the presence of the load. Dynamic coupling between the Dutch roll and a lateral load mode has been shown to decrease the Dutch roll damping. A more recent study of (Cicolani, Kanning & Synnestvedt, 1995) developed a comprehensive approach for slung-load modelling where generic simulation models for a tandem helicopter capable of carrying load in single or multiple points with one, two or more helicopters were investigated. (Fusato, Guglieri & Celi, 2001) developed a body-flap-lag model to study the flight dynamics of a single-rotor helicopter carrying a single-point suspended load, showing that the load affects trim primarily through the overall increase in the weight of the aircraft; the influence of cable length was negligible. (Stuckey, 2002), using the equations of motions developed by (Cicolani, Kanning & Synnestvedt, 1995) and an open-loop control for pilot modelling, developed a piloted simulation model for a tandem helicopter capable of carrying a mixed density slung loads. (Tyson, 1999) developed a slung-load simulation model composed on the GenHel UH-60 model and validated against flight test data. (Chen, 1998) built a non-linear simulation model for one rotor helicopter-slung system and investigated the sudden load movement causing the cables to slacken or collapse. (Kendrick & Walker, 2006), using the motion simulator at The University of Liverpool, investigated the stability and handling qualities of a single-rotor helicopter carrying a slung load showing that at hover and low speed the pilot found it easier to fly the helicopter with external load due to the increased damping in pitch provided by the load. (Bisgaard, 2006) developed an intuitive and easy-to-use way of modelling and simulating different slung load suspension types by using a redundant coordinate formulation based on Gauss' principle of Least Constraint using the Udwadia-Kalaba equation.

(Van der Kamp et al., 2005) (Reijm, Pavel & Bart, 2006) and (Pavel, 2010) investigated whether the three-strop suspension system – usually used to transport large loads (see right-hand side in Fig. 1) can be safely replaced by a two-strop suspension. A three-strop suspension system is actually a two-strop suspension backed up by a third point, the so-called 'redundant HUSLE'. The redundant HUSLE is a redundant set of slings which comes into action if one of the normal strops fails. However, such a system is expensive in terms of both money and time. Therefore, questioning how reliable the two-strop suspension was when compared to the three-point suspension; the above references concluded that although, in general, flying with the redundant HUSLE resulted in less violent helicopter reactions after load failure, redundant HUSLE did not necessarily mean safer. More

specifically, they demonstrated that loads up to only two tonnes could be safely suspended only in two-points without the need of using redundant HUSLE.

One of the many features of the CH-47 is its automatic flight control system AFCS. The goal of this chapter is to implement an advanced flight control system (AFCS) replicating the longitudinal axis AFCS of a Chinook CH-47D and use this system switched on to determine how the AFCS influences the recovery prospects of the Chinook helicopter after a front suspension failure. The chapter is structured as follows:

- The first section describes the AFCS characteristics;
- The second section develops the control laws for a longitudinal AFCS with pitch attitude hold and airspeed hold;
- The third section simulates an example of a failure scenario flown and determines the AFCS effects for recovering;
- The fourth section defines safety envelopes as boundaries of the maximum helicopter forward velocity achievable when recovery is possible after a load failure as a function of the load mass that can be safely transported;
- Finally, general conclusions and potential further extension of this work are discussed.

1.1 Tandem helicopter control

The pilot controls of a tandem helicopter are essentially the same as those for normal helicopters. A pilot has a stick to control longitudinal and lateral motion, a collective stick for thrust and pedals to control the yaw motion. However, the connections between controls and rotor hub angles are different. Collective input moves both swash plates equally up and down. Whereas a normal helicopter longitudinal control input tilts the swash plate longitudinally, this input results in differential collective in a tandem helicopter. Lateral motion is achieved by tilting both front and rear rotor in the same direction. The tail rotor that is used for yaw control, is missing. This function is replaced by lateral cyclic in opposite direction for front and rear rotor disc. It should be noted that pitch attitude is not only controlled by differential collective of the front and rear rotor heads. In the past many tests have been conducted in order to achieve acceptable pitch control. The first Piasecki tandem helicopter and the Bristol 173 (see Fig. 2) had longitudinal cyclic, both were either uncontrollable or could only fly backwards (Prouty, 2001). Therefore a later Piasecki model, the HRP-1 used differential collective for longitudinal control.



Fig. 2. Bristol 173 with cyclic pitch longitudinal control, Piasecki HRP-1 with differential pitch, www.aviastar.org

This type of helicopter control implies that with increased velocity the thrust of both rotors has to be tilted forward to compensate for the higher helicopter body drag. The lack of longitudinal cyclic in the HRP-1 forced the pilot to apply initially more differential thrust. This introduced an increase in nose down pitch angle. As a result of this forward helicopter pitch angle, the drag of the helicopter increases dramatically (see Fig. 3 from (Prouty, 2001)) To compensate for the large pitch angle, the longitudinal stick of the Chinook CH47-D controls differential thrust. Longitudinal cyclic is controlled separately by airspeed, keeping the helicopter body in acceptable pitch angles, thus minimizing helicopter body drag.

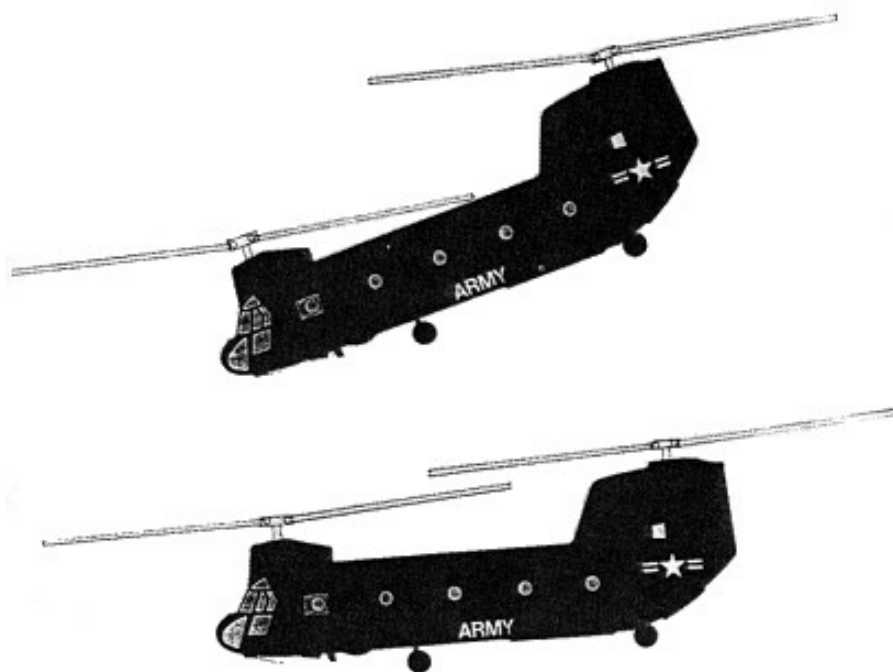


Fig. 3. Tandem helicopter with only differential pitch (top) and with differential collective and longitudinal cyclic pitch (bottom), (Prouty, 2001)

2. Description of the Chinook Automatic Flight Control System

An Advanced or Automatic Flight Control System (AFCS) employs the aerodynamic control surfaces to manipulate the forces and moments of an aircraft to control its velocity, attitude and position. The AFCS can do this with or without assistance from the pilot. The performance of the AFCS is largely governed by its flight control laws that translate the input of various sensors to control surface output. Just like the complete system, the design of these control laws, especially for military aircraft, is determined by the requirement to provide good handling qualities, over a wide range of operating conditions (including cargo transport), with a low pilot workload, while being easy to expand or modify.

For the Chinook helicopter, pilot control is done by varying the pitch of the blades either cyclically or collectively. This is done with the thrust control lever (collective), a cyclic control stick and the directional pedals, which are all coupled between the pilot and the co-

pilot's position. The stick and pedal movements are transferred with a system of bell-cranks, push-pull tubes and actuators to a control mixing closet, located in the small hallway connecting the cabin to the cockpit. In this mixing unit, the pilot control inputs are combined with the signals from the AFCS computers and then mixed to result in the required lateral cyclic and collective pitch of the two rotors.

Earlier models of the CH-47 only had a Stability Augmentation System (SAS) installed to assist the pilot in attitude stabilization. With the D-version, the AFCS was added, which brought a number of modifications and additions to the SAS. Still, the main objective remains attitude stabilization, including rate damping, of the helicopter about all three axes. However, it is extended with a number of features, that for example maintain the desired value of certain flight parameters such as airspeed, pitch attitude and bank angle. The CH-47F is to be the first of the Chinook family equipped with a digital AFCS (DAFCS), granting it Level I handling qualities and meeting the stringent ADS-33 requirements for operation in degraded visual environments. A few of its impressive features include position adjustment with 30 cm increments, automatic hover capture when the cyclic stick is released below 8 kts ground speed and an altitude hold mode that eliminates drift (Einthoven et. Al., 2006). Since the flight control actuation on the F-version remains unchanged from the D-version, the control system still contains mechanically linked actuators. Hence it does not qualify for the term fly-by-wire: this notion originated from the replacement of mechanical linkages by electric signalling.

The main features of the AFCS system as implemented in the Chinook version D consist of (Boeing Helicopters, 2004):

- Pitch attitude and long term airspeed hold, taking the position of the longitudinal cyclic stick as a reference;
- Long term bank angle and heading hold in level flight, bank angle hold in turning flight (performing coupled turns);
- A stable positive longitudinal stick gradient throughout the entire flight envelope;
- Fine adjustment of bank angle and airspeed trim (Vernier beep trim);
- Altitude hold by means of barometer or radar signals (this mode is valid in the CH 47D of the US Army; the Royal Netherlands Air Force replaced this mode by Flight Director);
- Improved manoeuvrability with the use of control position transducers for all cockpit controls;
- Electronic detent switching on lateral stick and pedals based on signals supplied by the AFCS;
- Longitudinal cyclic trim scheduling and automatic LCT positioning to ground mode when the aft wheels touch the ground;
- Use of the HSI bug error (error between actual and desired heading, indicated by a small token on the HSI instrument) for heading select (only in the CH 47D of the US Army; the Royal Netherlands Air Force replaced this mode by Flight Director);

Fig. 4 presents the cockpit interior of a CH-47D. Looking at this figure one can identify: 1) the AFCS control panel; 2) co-pilot pitch-roll control (cyclic stick); 3) pilot thrust control; 4) AFCS computer; 5) co-pilot multifunction display MMFD; 6) instrument panel; 7) centre console; 8) pilot pitch-roll control (cyclic stick); 9) multifunction display (AVMFD).



Fig. 4. Cockpit interior of a CH-47D, (Boeing Helicopters, 2004)

Regarding the AFCS of a CH-47D, this consists of the following parts:

- A cockpit control panel
- Two AFCS computers
- Three integrated lower control actuators (ILCA's)
- Two differential airspeed hold actuators (DASH)
- Two Longitudinal Cyclic Trim actuators (LCT)
- Attached to the cockpit controls are 2 magnetic brakes for yaw and roll, a longitudinal cockpit control driver actuator (CCDA) and a collective CCDA
- Three control position transducers (CPT's)

The AFCS cockpit control panel (number 1 in Fig. 4) contains 7 switches to control the many AFCS functions (see Fig. 5). On top, the flight director coupling switches that when pressed engage the coupling between the AFCS and the Flight Director. Only one flight director may be coupled at a time. The left lower side contains the switches that control the cyclic trim actuators. Normally the longitudinal cyclic trim (LCT) actuators are automatically operated by the AFCS computers, with computer 1 controlling the forward LCT and computer 2 governing the aft LCT actuator according to the LCT trim schedule. When the switch is flipped to manual setting, the pilot is able to independently direct the extension or retraction of both actuators. The AFCS system select switch can be found on the lower right side of the display. Usually both AFCS systems will be selected. When one AFCS system is switched

off, the Flight Director coupling and LCT functions continue to operate. The latter even keeps working with neither AFCS in operation.

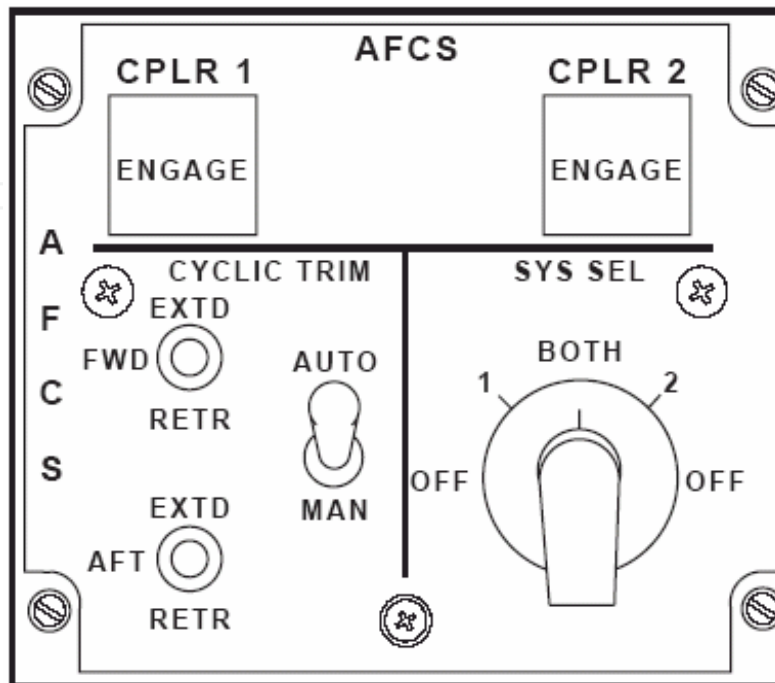


Fig. 5. AFCS control panel scheme, (Boeing Helicopters, 2004)

Two AFCS computers are located in the avionics compartment. Since the AFCS is a redundant system, in normal operation, each computer controls half of the input to the flight controls. This is described as “operation at half gain and half authority”. Failure of one of the computers results in the other computer taking over at $\frac{3}{4}$ gain but like regular operation, it has only up to half of the maximum travel of the working system available. In that case the remaining system is said to function at $\frac{3}{4}$ gain and half authority (Anon., 2002). When operational, the computers receive flight data from sensors and convert this into command signals that are fed to the actuators. Each unit directs its signals to the actuators according to a different path. Each actuator provides a position feedback signal to the related AFCS computer.

The Integrated Lower Control Actuators (ILCA) (see Fig. 6(a)) span 3 channels: pitch, roll, yaw. They separate the pilot control forces from the forces required to move the swashplates, which are generated by the upper controls. The ILCA's consist of two parts: a lower boost actuator and a dual extensible link. The hydromechanical lower boost actuators assist the pilot in controlling the helicopter. They are mechanically linked to the cockpit controls and will extend or retract in response to pilot inputs. The hydroelectrical dual extensible links incorporate an upper link, controlled by AFCS computer 1, and a lower link, driven by computer 2. This means that for full travel (full authority) both computers have to supply input. The actuating cylinders move solely based on AFCS commands without any corresponding cockpit controller motion. In the case none of the AFCS computers are working, the extensible links act as rigid links. The thrust input is enhanced with a lower boost actuator without extensible links, thereby assisting the pilot in moving the thrust control without providing a hydroelectrical input for the AFCS.

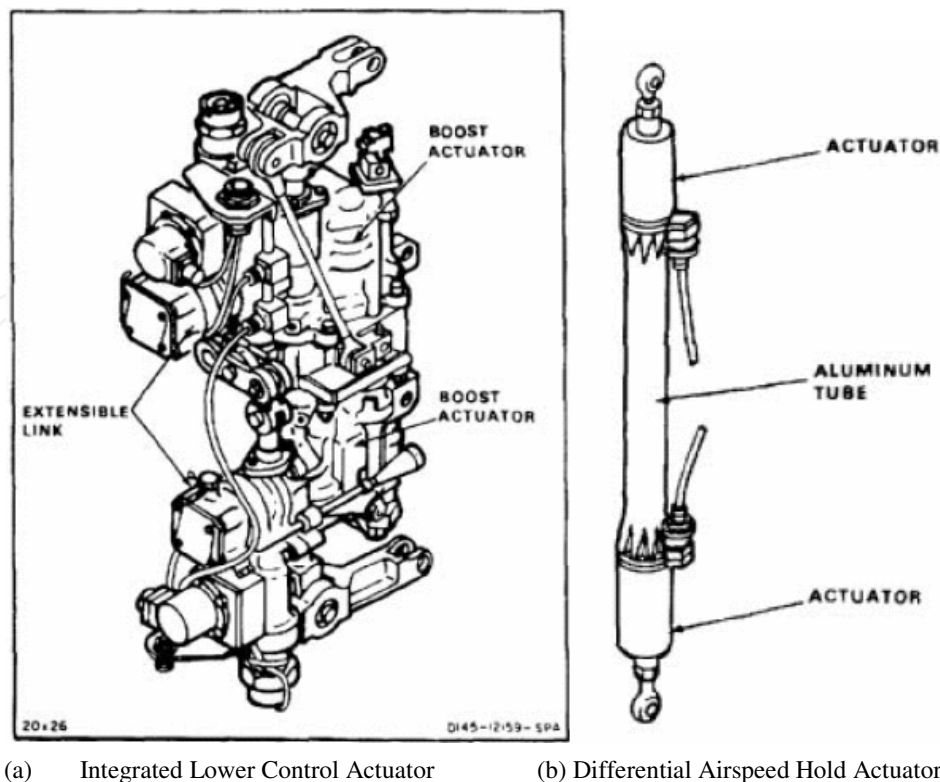


Fig. 6. Chinook actuators connected in series to cockpit controls (Anon, 2002)

The differential airspeed hold (DASH) actuator (see Fig. 6(b)) is installed between the cyclic stick and the pitch ILCA. The actuator is in fact a combination of two electro-mechanical linear actuators mounted end to-end inside a tube. Like an ILCA, the upper half is controlled by AFCS No. 1, the lower half by No. 2, so again both AFCS computers are required for full authority, which is equal to 50% of the longitudinal control range, taking about 5 seconds to complete full travel. The DASH extends and retracts with the purpose of long term stabilization of the pitch axis, arranging a positive stick gradient and maintaining airspeed about a fixed stick position. Its performance depends on the mode of operation, of which there are three:

- A normal mode in which it stabilizes 1) the airspeed when flying faster than 40 kts and 2) the pitch attitude at speeds below 40 kts.
- A Differential Collective Pitch Trim (DCPT) mode. This is turned on in special conditions such as high cyclic stick rate, large pitch attitude or on the ground. This is to prevent an exaggerated response from the actuator that would occur in these instances with the DASH in normal mode.
- The transition mode. This mode is entered when the DCPT conditions do not apply anymore and the AFCS is engaged. The system switches to a low rate driver (20% of the normal rate), forcing the DASH actuator to return to its normal position corresponding to the airspeed. This avoids a step-like control input when the DASH resumes normal operation.

The two longitudinal cyclic trim (LCT) actuators installed under the swashplate have as primary task to minimize fuselage drag by reducing the nose down attitude as airspeed and altitude build up. To manage this, the AFCS transmits signals to the LCT actuators which in

turn increase the longitudinal cyclic pitch angle of the fore and aft rotor. This way blade flapping is also reduced, lowering stresses on the rotor shafts. The pilot can also manually select the LCT actuator positions.

3. Modelling the Chinook tandem helicopter and its Automatic Flight Control System

3.1 Modelling the Chinook tandem helicopter with external load

A general non-linear six degree-of-freedom (6-dof) rigid body model for a generic tandem helicopter was first developed for piloted simulations ((Van der Kamp et. Al, 2005, Pavel, 2010). In a general non-linear 6-dof model the helicopter motion is represented by three translations and three rotations around the body axes-system centred on the helicopter centre of gravity, see Figure A 1 in Appendix A. The helicopter is modelled by dividing it into main components (front rotor, rear rotor, fuselage, horizontal stabilizer, vertical fin) and summing up the contribution of each part to the general system of forces and moments. The following main assumptions were made: 1) Aerodynamic forces and moments are calculated using the blade element theory and integrating along the radius and azimuth to obtain their average effect; 2) The fuselage is modelled with linear aerodynamics; 3) Rotor disc-tilt dynamics (the so-called ‘flapping dynamics’) are neglected and only steady-state rotor disc-tilt motion is considered; 4) The dynamic inflows of both front and rear rotors are included in the model as state variables and can be described as a quasi-steady dynamic inflow by means of time constants of a value 0.1 sec; 5) The rotors are modelled with a centrally flapping hinge; 6) There are no pitch-flap or pitch-lag couplings; 7) The lead-lag motion of the blades is neglected; 8) The blades are rectangular; 9) There are no tip losses; 10) Gravitational forces are small compared to aerodynamic, inertial and centrifugal forces; 11) The flapping and flow angles are small; 12) The front rotor angular velocity is constant and anticlockwise, the rear rotor angular velocity is constant and clockwise; 13) No reverse flow regions are considered; 14) The flow is incompressible; 15) The blades have a uniform mass distribution; 16) The blade elastic axis, aerodynamic axis, control axis and centre of mass axis coincide; 17) The blades are linearly pre-twisted $\theta_{\text{twist}} = -9.14$ deg. For the expressions of the forces and moments acting on the helicopter components, the reader is referred to APPENDIX A. The equations of motion describing the motion of the helicopter in the 6-dof model are presented in APPENDIX A. To this model, a 6-dof model for the load has been added. The helicopter has three suspension points $i=1,2,3$ underneath its floor as seen in Figure A6, the tension force in one cable j being S_{ij} . The slings are modelled as linear springs without mass and it is assumed that they have small internal damping. The damping coefficient is set large enough to prevent the oscillating load from inducing a pendulum-like motion. In APPENDIX A more detail is given on the calculation of load sling forces (see eqns. (24) and (25)). The load is modelled as a 6-dof body, the helicopter slings being connected to the load as seen in Figure A7. The slings are modelled as linear weightless springs with a small internal damping. Appendix B presents the Chinook data for the helicopter and load.

3.2 Developing control laws for the longitudinal AFCS

Next, AFCS control laws for operating the Chinook helicopter are added to the presented flight mechanics model. In a classical AFCS, the computation of signals for stabilization,

control decoupling and automatic control of the helicopter take place. Generally, an AFCS comprises the sensors, the filters, the stability and control augmentation system (SCAS) and the autopilot which can completely take over the pilot in order to execute certain control tasks.

Fig. 7 (Reijm, Pavel & Bart, 2006) displays for example the pitch control laws connected to the generic helicopter model. Generally, the pitch control laws have 6 input paths: pitch attitude, pitch rate, yaw rate, bank angle, limited airspeed and the longitudinal control position. These signals arrive from the gyros, CPT and pressure sensor and are manipulated to steer the pitch ILCA extensible links to provide pitch rate damping and the DASH actuator to maintain airspeed and a positive stick gradient. The actuation system is quite a complicated mechanism with its own feedback control designed to ensure that the response and stability to control inputs has good performance. Helicopters fitted with an AFCS usually incorporate a limited authority series SCAS actuators, The SCAS authority, i.e. the amount in which a SCAS can overrule the pilot is limited to amplitudes of $\pm 10\%$ of the full actuator throw. For this work, it is assumed that each actuation element can be represented as a first order lag, although this assumption is a crude approximation of the complex behaviour of the servo-elastic system.

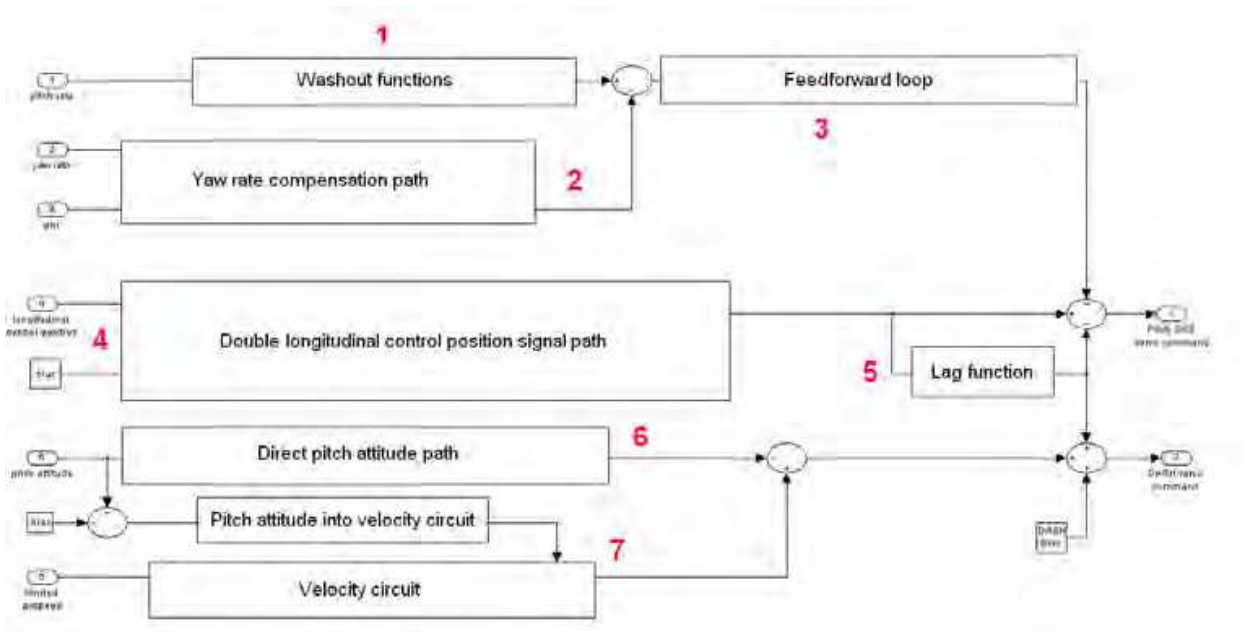


Fig. 7. Pitch control laws for the longitudinal AFCS (Reijm, Pavel & Bart, 2006)

Looking at Fig. 7, one can distinguish the various parts of the control laws. Starting with location 1, this is the primary input for the ILCA path: the pitch rate. It passes through washout functions which act like a sink and filter the signal for certain frequencies. These washout transfer functions can be tuned to select a desired filter strength and a frequency that should be eliminated from the signal. Moving to location 2, the filtered pitch rate signal is compensated by the yaw rate and roll attitude, presumable to cater for the effects of the coupling between the longitudinal and lateral flight dynamics. In location 3 the compensated

signal passes through a feedforward loop; the combination of a feedback and feedforward loop increase the responsiveness of a system, decreasing the time to return to the desired state after a disturbance. The longitudinal control position (location 4 in the figure) also contributes to the ILCA signal with the purpose of control augmentation. The CPT signals pass via a direct path and high gain path, which incorporates a *rate limiter*. The rate limiter constricts the appliance of the CPT signal to repress the effects of rapid stick movement, which could otherwise result in overreaction of the system. The direct and rate limited signals are summed and together form the resulting longitudinal CPT signal to be used for the ILCA and DASH actuator. Before the CPT signal reaches the ILCA, it is modified by a special construction involving the regular signal subtracted by the signal that has been filtered by a *lag function*. Generally, the task of a lag function is to cancel high frequency throughput to prevent saturation. They are defined by the transfer function $\frac{1}{\tau s + 1}$ in which τ is the time constant

that defines the effectiveness of the filter. The higher the time constant, the better is the capacity of filtering high frequencies. The time constant τ is typically between 25 and 100ms, giving actuation bandwidths between 40 and 10 rad/s/. For this study a time constant of 100ms was chosen, resulting in a system with lower actuation bandwidth which shows that the actuation inhibits pilot rapid control actions. Then at location 5 one can see the *washout circuit* designed to only produce output during the transient period, cancelling the steady-state throughput. This behaviour is exactly what is required for control augmentation: the assistance by the boost actuators should be generated only when the pilot is moving the stick, not when keeping it steady. The resulting longitudinal CPT signal not only directs ILCA extension, but also controls the DASH actuator. The signal is supplemented with the pitch attitude that enables pitch attitude hold (location 6). The pitch attitude also works as input for the velocity control circuit in location 7. This velocity control circuit enables the DASH system to provide a positive stick gradient, but also includes feedback and feedforward loops to act on attitude changes caused by gusts.

4. Simulating front cable failure scenarios

The generic control scheme of Fig. 7 is next implemented in the generic tandem helicopter + load model.

The generic helicopter/slung load model as presented above is used next to simulate failure scenarios of the front cable. A tandem V-shape suspended load is assumed to hang underneath the helicopter so that failure of the front hook means actually failure of the two front cables.

In analysing the pilot recovery chances after a front cable failure without dropping the external load, the following question arose: what happens if the remaining cables are not strong enough to carry the load and they snap so that the pilot loses the load. Therefore the tension in the remaining cables was analysed to determine the cases in which the pilot would lose the load. After a cable failure the tension in the remaining cables increases rapidly and may cause them to snap. The snapping of the other cables may cause extra piloting problems, even loss of control and a possible destruction of the rotor above. Generally, generic sling specifications demand a guaranteed life of four years. At the Beginning Of Life (BOL) they must withstand 7 times the designed tensile strength. At the end of their service or End Of Life (EOL) this number has dropped to a minimum of 4.2

times design strength, which is equal to the design strength of suspension points on the external loads. For the Chinook, the tensile strength are calculated with a design load of 17000lb (7.6x10⁴ N) for each cable/hook and 25000lb (11.1x10⁴N) for a combined fore and aft cable/hook (31). During the failure simulations it became clear that the tension in the cables is very high when recovering to normal flight. On many occasions the EOL strength was exceeded and sometimes the BOL strength as well. As it was difficult to decide when a sling reaches its ultimate/breaking strength and snaps, the actual snapping point was set to the BOL strength as this represented a worst-case scenario.

First, to fly the helicopter/slung load system in the front cable failure scenario, simple PID controllers have been developed to generate all control positions. Generally, in a PID controller, it is considered that the collective controls the altitude, the longitudinal cyclic controls pitch attitude, the lateral cyclic controls the roll motion and the pedal controls the sideslip, i.e.:

$$\begin{aligned} coll &= K_z (z_{req} - z) + K_{int_z} \int (z_{req} - z) dt + K_w w \\ long &= K_\theta (\theta_{req} - \theta) + K_{int_ \theta} \int (\theta_{req} - \theta) dt + K_q q \\ lat &= K_\phi (\phi_{req} - \phi) + K_{int_ \phi} \int (\phi_{req} - \phi) dt + K_p p \\ pedal &= -K_\psi \beta_{fus} + K_{int_ \psi} \int (-\beta_{fus}) dt - K_r r \end{aligned} \quad (1)$$

At the guidance level, the required pitch attitude is controlled by an altitude hold controller and the required roll angle is controlled by a lateral position hold controller.

$$\begin{aligned} \theta_{req} &= K_h (h_{req} - h) + K_{int_h} \int (h_{req} - h) dt + K_{h\dot{dot}} \dot{h} \\ \phi_{req} &= K_y (y_{req} - y) + K_{int_y} \int (y_{req} - y) dt + K_{y\dot{dot}} \dot{y} \end{aligned} \quad (2)$$

The longitudinal and lateral pilot inputs are mixed at the level of swashplate as given in (Ostroff, Downing and Rood, 1976).

$$\begin{aligned} \theta_{1cf} &= \theta_{1cf,pilot} \cdot \cos \beta_{fus} + \theta_{1sf,pilot} \cdot \sin \beta_{fus} \\ \theta_{1sf} &= \theta_{1cf,pilot} \cdot \sin \beta_{fus} - \theta_{1sf,pilot} \cdot \cos \beta_{fus} \\ \theta_{1cr} &= \theta_{1cr,pilot} \cdot \cos \beta_{fus} + \theta_{1sr,pilot} \cdot \sin \beta_{fus} \\ \theta_{1sr} &= -\theta_{1cr,pilot} \cdot \sin \beta_{fus} + \theta_{1sr,pilot} \cdot \cos \beta_{fus} \end{aligned} \quad (3)$$

Next, the initial PID controlled model is replaced with the longitudinal AFCS controlled system of Fig. 7, the other inputs remaining still PID controlled. This new pilot model is used to simulate different failure scenarios of the front cable. The following steps are taken to complete a failure scenario with the longitudinal AFCS switched on:

- Calculate the trim state for a desired airspeed;
- Use Bilinear Transformation to map the continuous time transfer functions to the discrete domain;

- Compute the new pilot input value for smooth transition;
- Simulate the first 25 seconds with a full PID control. This is done because when the AFCS is turned on in flight after it has been switched off, or it leaves ground mode, a DASH error signal could exist. This means that DASH actuator operation and the longitudinal stick position are out of sync, requiring a small period of time for the actuator to cancel the error signal after which it is able to resume normal operation. This is done with the Transition Mode of the DASH. Discussions with RNLAF test pilots provided the indication that approximately 25 seconds is a realistic value;
- At 25 seconds, switch to longitudinal AFCS with all other inputs (collective, lateral and pedal) PID controlled;
- At $t = 26$ seconds, a cable failure will be introduced. The control laws will keep operating, immediately responding to the changing helicopter states.
- From the start of the failure until the specified pilot reaction time of either 0, 1 or 2 seconds, the PID controllers will enter a stick-fixed mode, remaining at the position they were in at $t = t_{\text{failure}}$.
- When the reaction time period has expired, the PID controllers will kick in and the simulation will again run in mixed mode until it is finished, covering the same 5 seconds from $t = t_{\text{failure}}$.

To determine the limits within which the pilot can control the recovery, the ADS-33 standard (ADS-33, 2000), section 3.1.14.4 ‘Transients Following Failures’ has been used. According to ADS-33, for rotorcraft without failure warning and cueing devices, the perturbations encountered shall not exceed the limits as given in Table 1 (equivalent with Table III from ADS-33). Also, according to pilot experience it appeared that the pilot can react within 1 or 2 seconds after the load failure. Therefore, the pilot reaction time in the simulations performed in this paper has been adjusted to 1 and maximum 2 seconds.

Level	Flight condition		
	Hover and Low speed	Forward Flight	
		Near-Earth	Up-and-away
1	3° roll, pitch, yaw 0.05g n_x, n_y, n_z No recovery action for 3.0 sec	Both Hover and Low Speed and Forward Flight Up-and-Away requirements apply	Stay within OFE. No recovery action for 10 sec
2	10° attitude change 0.2g acceleration No recovery action for 3.0 sec	Both Hover and Low Speed and Forward Flight Up-and-Away requirements apply	Stay within OFE. No recovery action for 5.0 sec
3	24° attitude change 0.4g acceleration No recovery action for 3.0 sec	Both Hover and Low Speed and Forward Flight Up-and-Away requirements apply	Stay within OFE. No recovery action for 10 sec

Table 1. Transients following failures (ADS-33, 2000)

A typical failure simulation can be seen in Fig. 8. The case considered is the helicopter flying forward at 50 kts when a front failure occurs with a 2-point suspended load of 2 tonnes. It is considered that the pilot reaction starts 1 sec after the failure. The controls remain unchanged from the moment of failure to the moment of pilot reaction (i.e. for 1 second). Looking at this figure it appears that the pilot can control this failure, being close to the upper limit for the longitudinal controller and well within the limits for the collective and lateral controllers.

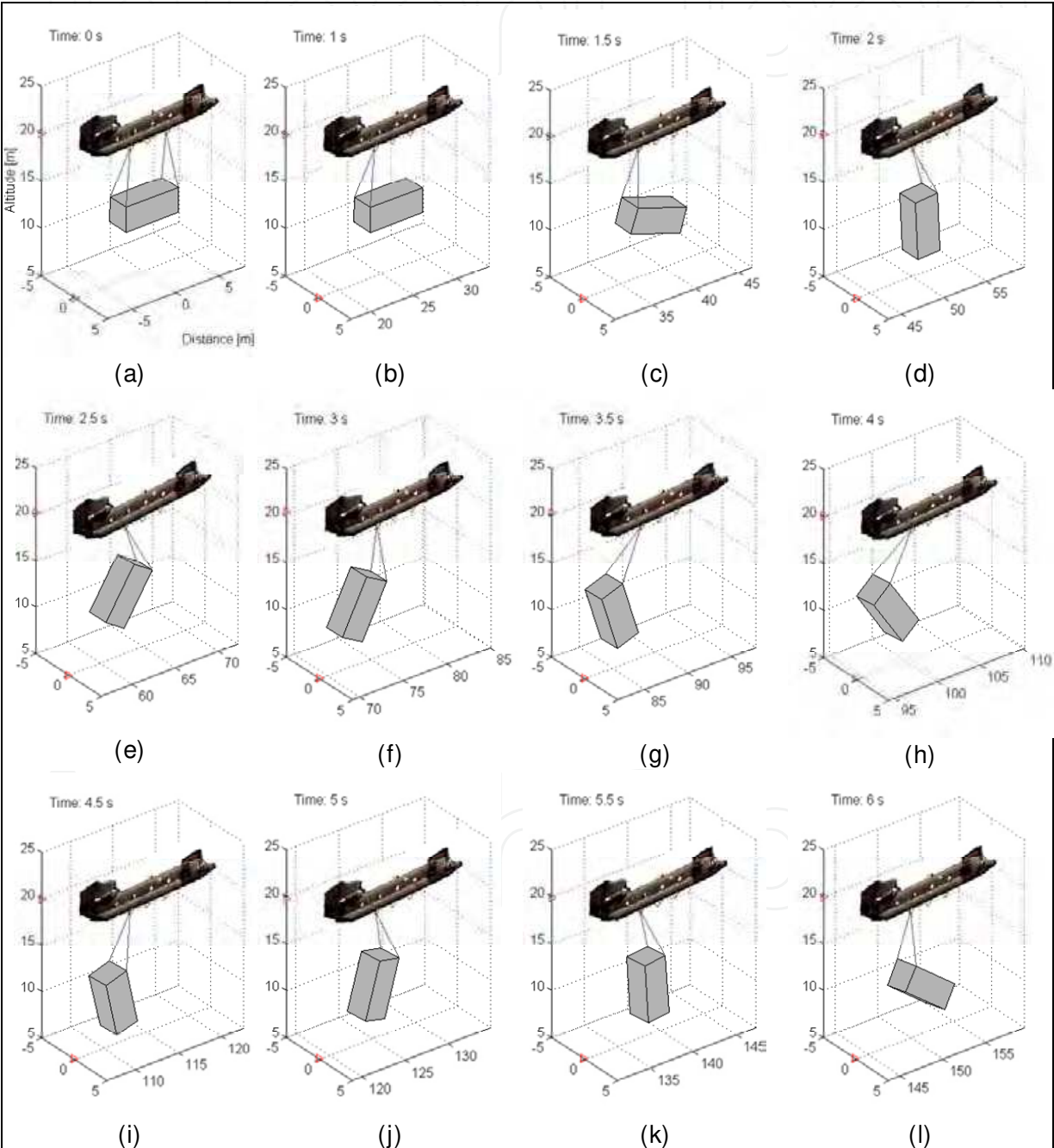


Fig. 8. Helicopter and load snapshot to a front cable failure scenario from 50 kts initial velocity, 2-point suspension, 2000 kg load, 1 sec delay in pilot reaction

Concerning the time responses of the servo commands control actions, Fig. 9 displays the pitch control law of the actuator servo commands during a 30-second level flight at 50 kts.

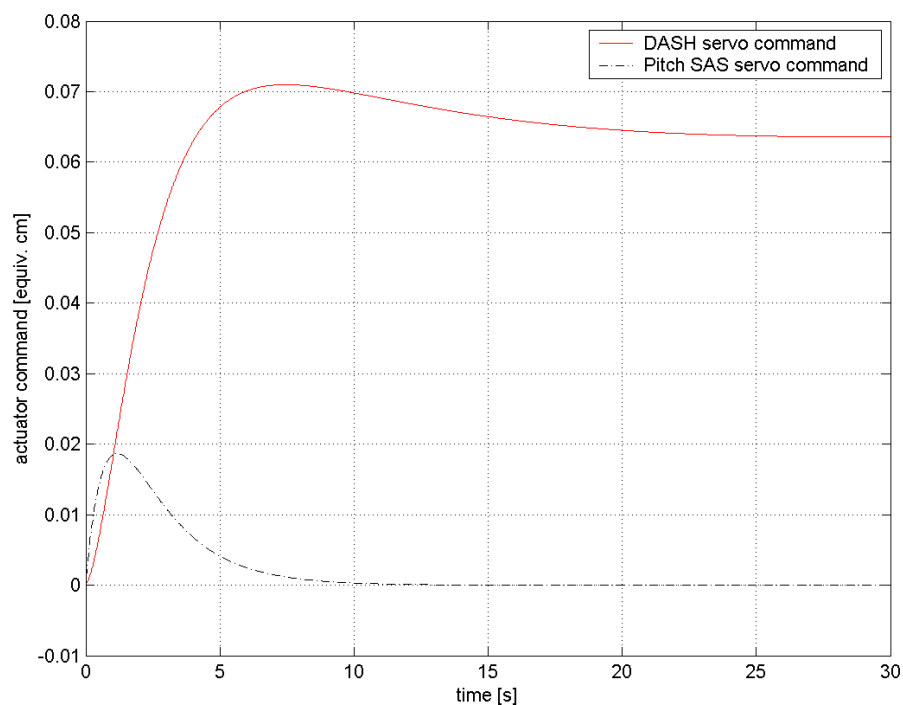


Fig. 9. Pitch control law for the DASH and SAS actuator command during the 50 kts forward flight

Looking at this figure, one can see that there is a 25-second settling time that the DASH actuator requires before reaching a steady state value of about 6.3 cm.. Such behaviour seems to agree with the RNLAf CH-47D flight manual ((Anon, 2004),section 8.3). The manual states that when the AFCS is turned on in flight after it has been switched off, or it leaves ground mode, a DASH error signal could exist. This means that DASH actuator operation and the longitudinal stick position are out of sync, requiring a small period of time for the actuator to cancel the error signal after which it is able to resume normal operation. This is done with the Transition mode of the DASH as described above. The manual does not mention how long this period actually lasts, but, from discussions with Chinook pilots, it appears that this period it would amount to approximately 25 seconds, value similar to the one encountered in Fig. 9.

Furthermore, the following scenarios are considered:

- the load is suspended on two-point or three-point suspension systems. In the three-point suspension the redundant set of slings (between the front and rear hook) come into action when the front cables fail.
- the load can be suspended either in a nose-down position (so-called 'nose-down rigged load') or in a horizontal position (so-called 'level rigged load').
- the helicopter is flying initially in level flight at velocities varying between 10 and 100 kts
- the helicopter can carry three different container of 2 tonnes, 6 tonnes or 10 tonnes.
- the pilot reaction time to failure varies from instantaneously reaction (ideal case) to a delay in response of 1 and 2 seconds.

Fig. 10 shows the helicopter pitch rate, attitude and velocities after a cable failure in the case of a PID controlled helicopter (left hand side of the figure) and an AFCS controlled helicopter (right hand side). The case considered is the helicopter flying forward at 50 kts when a front failure occurs with a 2-point suspended load of 2000 kg. It is considered that the pilot PID control will start to react at 1 sec after the front suspension point has failed. The controls remain unchanged from the moment of failure to the moment of pilot reaction (i.e. for 1 second). It is interesting to discuss how the AFCS affects the simulation. While the PID controller is restrained by the pilot reaction time, the AFCS control laws immediately start reacting to the change in helicopter pitch attitude caused by the swinging of the load. This should result in a lower maximum pitch rate, an expectation confirmed by the results. The maximum pitch rate q_{max} of the PID controlled helicopter is equal to 8.6 deg/sec (27th second), whereas the q_{max} resulting from AFCS control comes to 7.6 deg/sec (2nd second), an 11% attitude reduction. Concerning the pitch attitude, one can see that the AFCS controller clearly has trouble to maintain the trimmed pitch attitude, allowing it to increase to 8 degrees. This immediately has its effect on the forward velocity that begins to decline as soon as the pitch angle starts to build up at about 27 seconds. The filtering of the pitch attitude control also has its effect on the vertical velocity, but this is neither vital to the survival of the helicopter nor relevant to the ADS-33 handling limits. Simulating different scenarios it was observed that the DASH control circuit fails to maintain airspeed when flying faster than 40 kts. Though it appears more and more likely that the implementation of the DASH control circuit does not wholly agree with the real-life situation, the pitch ILCA is still doing its job just as intended, keeping the pitch rate within handling limits and making recovery possible.

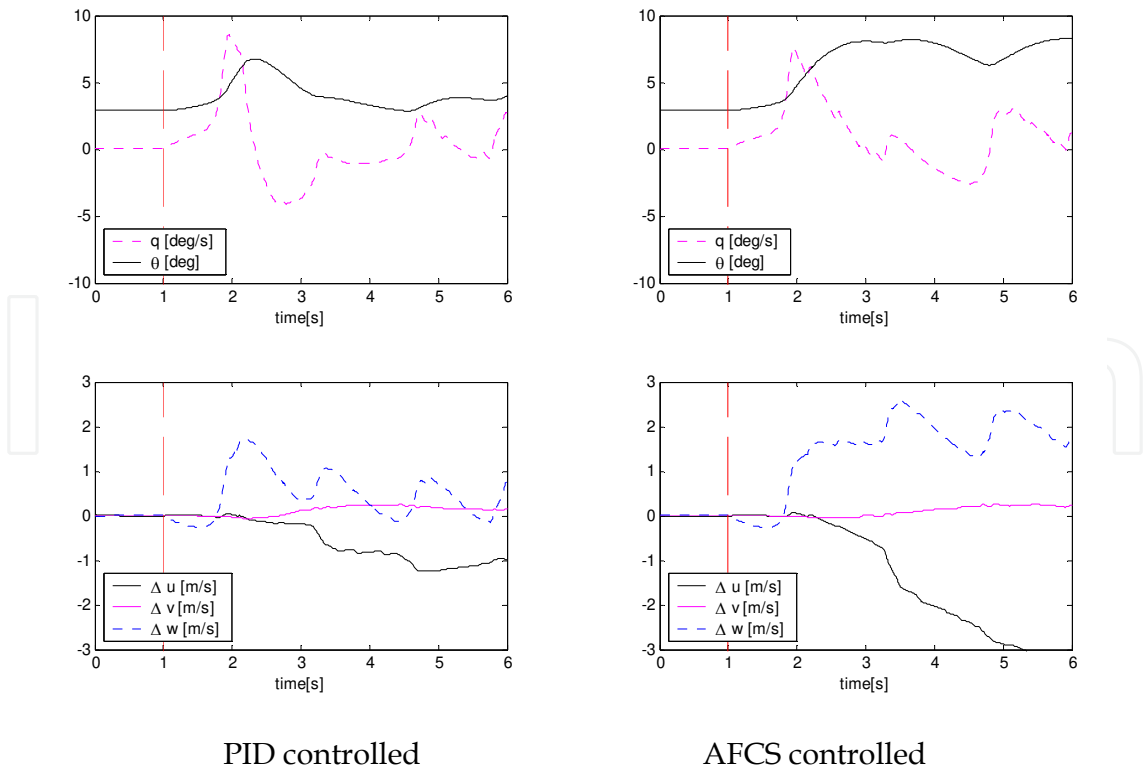


Fig. 10. Helicopter motion after front suspension load failure, 50kts, two-point suspension, 2 tonne mass load

Fig. 10 clearly shows the advantage of the running AFCS: the pitch ILCA picks up on the increasing pitch rate right after the cable failure, resulting in a lower maximum pitch rate compared to PID control with a one second reaction time delay. The PID controlled pitch rate ranges from -4 to +8 deg/s, the AFCS improves on this with a range of -2.5 to +7.5 deg/s.

The difference in helicopter motions result in a small difference in the way the load swings. But surprisingly, the change is not to be found in the axis in which the controller actually differs. Fig. 11 presents the pitch, roll and yaw motions of the container. Apart from the deviation in shape, the longitudinal AFCS controller causes an increased negative load roll rate and larger overall yaw rate amplitude. The swinging of the load may even result in a destructive collision between the container and helicopter hull before the load can be safely detached. This danger should be investigated in future research.

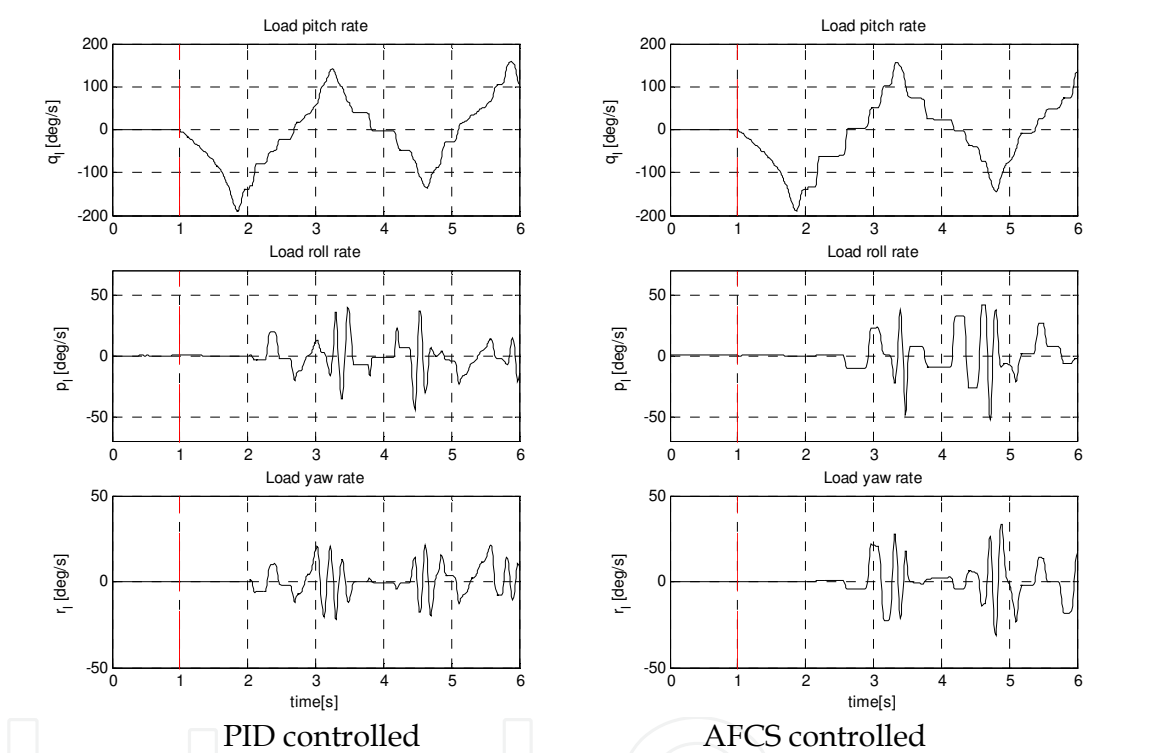


Fig. 11. Load motion after front suspension cable failure

5. Defining safety envelopes for the load failures

The numerous failure scenarios simulated have been plotted in safety envelopes giving the velocity when recovery was possible as a function of load mass carried. Fig. 12 and Fig. 13 present the envelopes for a two- and respectively three-point suspension level rigged container after the front suspension point failed as a function of pilot reaction time to recover. Two controls are analysed: (a) a PID controller and (b) an AFCS controller. Looking at Fig. 12 one can see that in case of a two-point suspension, the PID control covers a larger envelope area than the partial AFCS control when the pilot reacts instantaneously to the failure ($\tau=0$ sec). However, in case of a three-point suspension this difference is not present. Fig. 12(b) shows a kind of inverse trend in safety when switching on the AFCS: if the pilot reacts instantaneously to the failure ($\tau=0$ dotted line envelope) he has less chances to recover

than if he reacts one second later ($\tau = 1\text{sec}$ point dotted line). This can be explained as follows: the AFCS is actually first attempting to converge to reference (trim) values. If the pilot reacts immediately to the failure, the AFCS has difficulties in combining pilot inputs with its own convergence algorithm. But as soon as the circumstances favour the AFCS controller, i.e. the pilot reaction time becomes 1 or 2 seconds, the advantage of its application becomes clear.

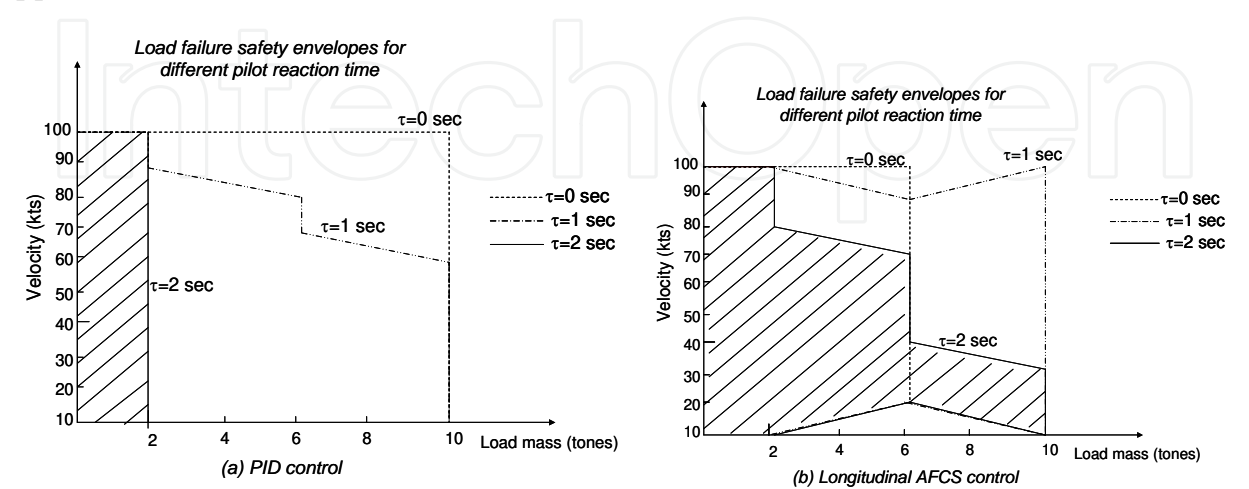


Fig. 12. Safety envelopes for a two-point suspension

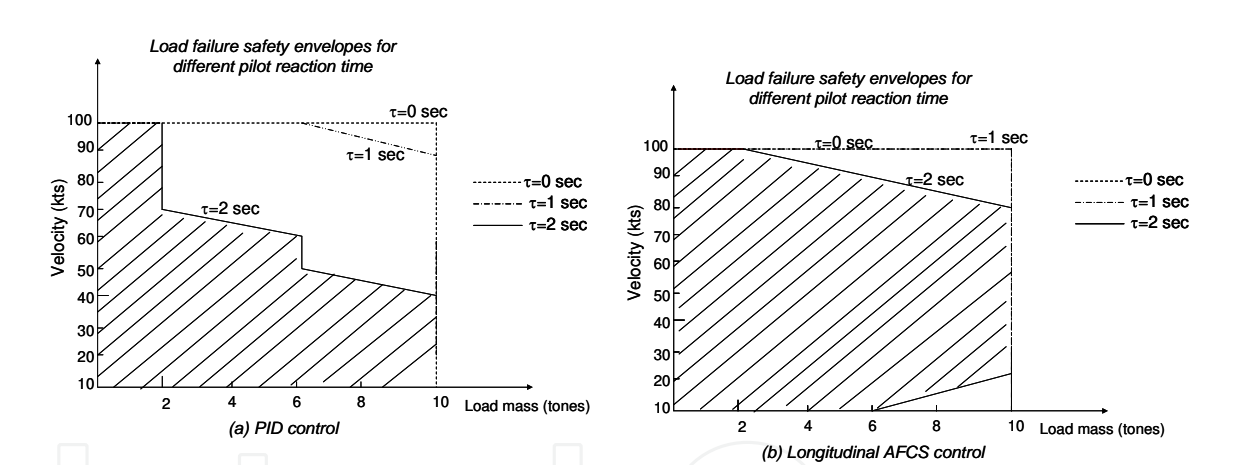


Fig. 13. Safety envelopes for a three-point suspension

Especially with a 2 second reaction time the contribution of the AFCS to the helicopter recovery emerges as invaluable. This can be seen when comparing Fig. 12(a) with Fig. 12(b), showing even more than doubling the envelope area when $\tau=2$ sec and when instead of using PID controller the AFCS is switched on. This means that, when compared to a basic PID controlled helicopter, the AFCS is offering a much broader flight regime in which under slung loads can be transported. While the PID only stabilizes the helicopter motions by limiting the rate at which the attitude changes, the AFCS is attempting to converge to trim values.

Comparing the two-point and three-point suspension for an AFCS controlled helicopter (i.e. Fig. 12(b) with Fig. 13(b)) it appears that a three-point suspension is safer. However, this does not mean that the two-point suspension is not safe for a certain condition. For example, if a 6 tone load needs to be transported, one can choose for a two-point suspension with the condition of not exceeding 70 kts in level flight. Above this velocity the chance to recover in

case of a load failure is questionable. In case of a 10 tones load, the AFCS for a two-point suspension cannot contribute to the pilot efforts to recover the load if the failure occurs above 30 kts. In this case it is safer to choose a three-point suspension for load transportation.

6. Conclusion

The purpose of this chapter is to determine how the AFCS influenced the recovery prospects of a Chinook helicopter with an external sling load when one of its cables brakes. This can be of vital importance for deciding whether to replace the safer three-point redundant suspension to a two-point suspension during Royal Netherlands Air Force operations. The chapter presented the flight control laws for a longitudinal automatic flight control system (AFCS). The general conclusion that could be drawn was that the assistance of the AFCS expanded the number of occasions at which the helicopter motions stayed within the handling limits during recovery of a cable failure. In many cases, the AFCS cancelled the negative effect of a delayed pilot response, supporting the supposition that the combination of active pilot control and AFCS backup could push the flight envelope boundaries even further. The chapter proposed safety envelopes covering the areas that define the conditions at which a cable failure at a suspension point could happen without presumable fatal consequences. It was demonstrated that since the longitudinal part of the AFCS was operating continuously, it was not bound by the obstruction of the imposed pilot reaction time. For this reason, partial AFCS control gained an advantage when the pilot reaction was delayed. Flying with a two-point suspension is just as safe as a three-point suspension stipulating that the safety envelope boundaries are obeyed.

7. Appendix A

7.1 Derivation of the equations of motion in a six degree-of-freedom model

In a general 6-dof non-linear body model the helicopter motion is represented by three translations and three rotations around the body axes-system $\bar{E}_B \{X_B \ Y_B \ Z_B\}$ centred in the helicopter centre of gravity, see Fig. A1.

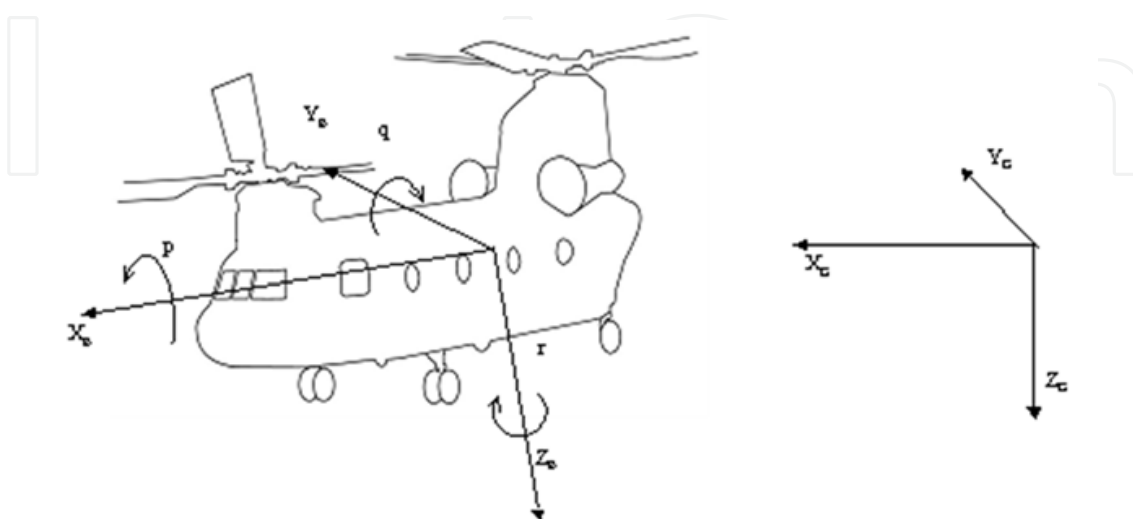


Fig. A1. System of coordinates used to express the helicopter motion in the 6-dof model

The system of equations describing completely the motion of the helicopter in an inertial system are:

$$\begin{aligned}
 \dot{u} &= -g \sin \theta + \frac{X}{m} + rv - qw \\
 \dot{v} &= g \sin \phi \cos \theta + \frac{Y}{m} - ru + pw \\
 \dot{w} &= g \cos \phi \cos \theta + \frac{Z}{m} + qu - pv \\
 \dot{p} &= \frac{rq(I_y I_z - I_z^2 - I_{xz}^2) - pq I_{xy}(I_x - I_y + I_z) + I_z L + I_{xz} N}{I_x I_z - I_{xz}^2} \\
 \dot{q} &= \frac{M + pr(I_z - I_x) + I_{xz}(r^2 - p^2)}{I_y} \\
 \dot{r} &= \frac{-rq I_{xz}(I_x - I_y + I_z) + pq(I_x^2 - I_x I_y + I_{xz}^2) + I_{xz} L + I_x N}{I_x I_z - I_{xz}^2} \\
 \dot{\psi} &= \frac{(q \sin \phi + r \cos \phi)}{\cos \theta} \\
 \dot{\theta} &= q \cos \phi - r \sin \phi \\
 \dot{\phi} &= p + \dot{\psi} \sin \theta
 \end{aligned} \tag{4}$$

In order to describe completely the helicopter motion w.r.t. the Earth system, the equations of trajectory can be added:

$$\begin{aligned}
 \dot{x} &= (u \cos \theta + (v \sin \phi + w \cos \phi) \sin \theta) \cos \psi - (v \cos \phi - w \sin \phi) \sin \psi \\
 \dot{y} &= (u \cos \theta + (v \sin \phi + w \cos \phi) \sin \theta) \sin \psi + (v \cos \phi - w \sin \phi) \cos \psi \\
 \dot{z} &= -u \sin \theta + (v \sin \phi + w \cos \phi) \cos \theta
 \end{aligned} \tag{5}$$

To these systems of equations, two differential equations are added for the dynamic inflow of the front main and rear rotors, describing the dynamic inflow as a “quasi-steady inflow” by means of time constants:

$$\begin{aligned}
 \tau_f \dot{\lambda}_{if} &= C_{T,Elem,f} - C_{T,Glau,f} \\
 \tau_r \dot{\lambda}_{ir} &= C_{T,Elem,r} - C_{T,Glau,r}
 \end{aligned} \tag{6}$$

where $C_{T,elem}$ and $C_{T,Glau}$ are the rotor thrust coefficients as expressed in blade element theory and respectively Glauert theory. The total forces and moments acting on the helicopter centre of gravity consist of the sum of front and rear rotors (with indices Rf and Rr), rotor torque (Q) and helicopter body aerodynamics (B). For the load, a suspension point component (S) is considered which is added when the load is attached underneath the helicopter model.

$$\begin{aligned} X &= X_{Rf} + X_{Rr} + X_B (+X_S) \\ Y &= Y_{Rf} + Y_{Rr} + Y_B (+Y_S) \\ Z &= Z_{Rf} + Z_{Rr} + Z_B (+Z_S) \\ L &= L_{Qf} + L_{Qr} + L_{Rf} + L_{Rr} + L_B (+L_S) \\ M &= M_{Rf} + M_{Rr} + M_B (+M_S) \\ N &= N_{Qf} + N_{Qr} + N_{Rf} + N_{Rr} + N_B (+N_S) \end{aligned} \tag{7}$$

The rotor forces and moments consist of front and rear vertical thrust components T_f and T_r , drag forces H_{Xf} and H_{Xr} , lateral forces H_{Yf} , and H_{Yr} and rotor shaft torques M_{Qf} and M_{Qr} as seen in Fig. A2.

$$\begin{aligned} X_{Rf} &= X_{Tf} + X_{Hf} & X_{Rr} &= X_{Tr} + X_{Hr} \\ Y_{Rf} &= Y_{Tf} + Y_{Hf} & Y_{Rr} &= Y_{Tr} + Y_{Hr} \\ Z_{Rf} &= Z_{Tf} + Z_{Hf} & Z_{Rr} &= Z_{Tr} + Z_{Hr} \\ L_{Rf} &= Y_{Rf}h_f - Z_{Rf}f_1 + L_{Qf} & L_{Rr} &= Y_{Rr}h_r - Z_{Rr}f_1 + L_{Qr} \\ M_{Rf} &= -X_{Rf}h_f - Z_{Rf}l_f & M_{Rr} &= -X_{Rr}h_r + Z_{Rr}l_r \\ N_{Rf} &= X_{Rf}f_1 + Y_{Rf}l_f + N_{Qf} & N_{Rr} &= X_{Rr}f_1 - Y_{Rr}l_r + N_{Qr} \end{aligned} \tag{8}$$

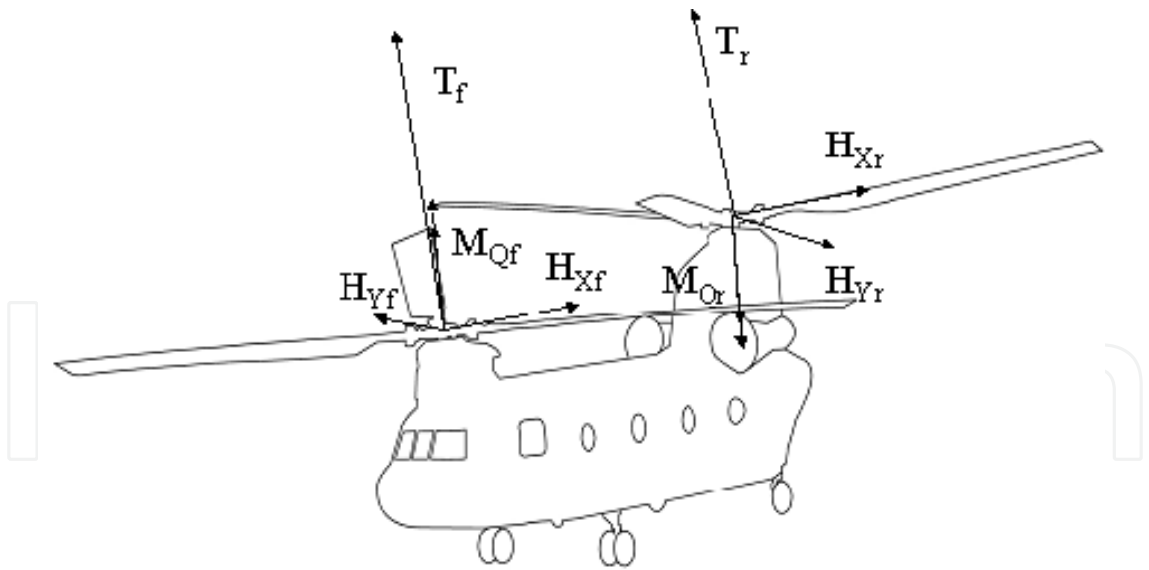


Fig. A2. Forces and Moments on the rotors

The model uses the following sign conventions (see Fig. A3 and Fig. A4): 1) Longitudinal disc tilt for front and rear rotors a_{1f} and a_{1r} are assumed positive for backward tilted rotor disc plane; 2) Lateral disc tilt for front and rear rotor b_{1f} and b_{1r} are positive for rotor disc plane tilted in the direction of azimuth angle $\psi=90^\circ$ (i.e. $b_{1f} > 0$ to the right and $b_{1r} > 0$ to the left, backside view); 3) Collective pitch for front and rear rotor θ_{0f} and θ_{0r} are positive when

the pilot moves the collective up; 4) Longitudinal cyclic for front and rear rotor θ_{1sf} and θ_{1sr} are assumed positive when the pilot moves the stick forward; 5) Lateral cyclic for front and rear rotors θ_{1cf} and θ_{1cr} are assumed positive when the pilot moves the stick to the right for cyclic pitch to the right.

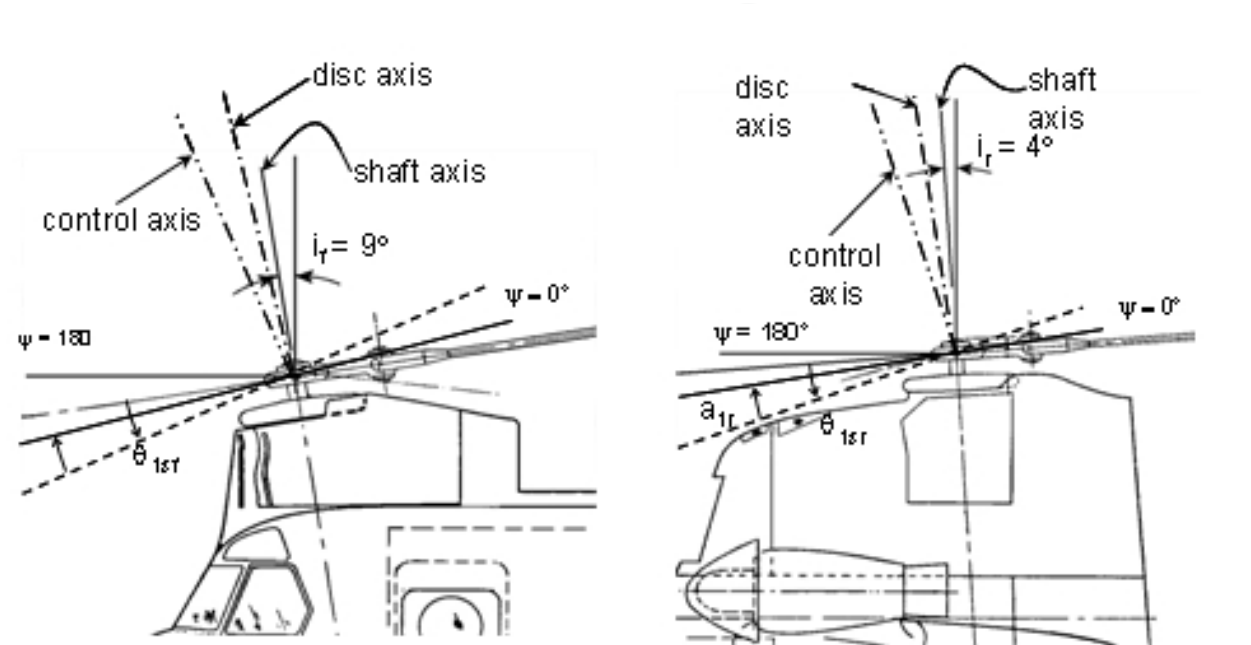


Fig. A3. Longitudinal axis Chinook control (side view)

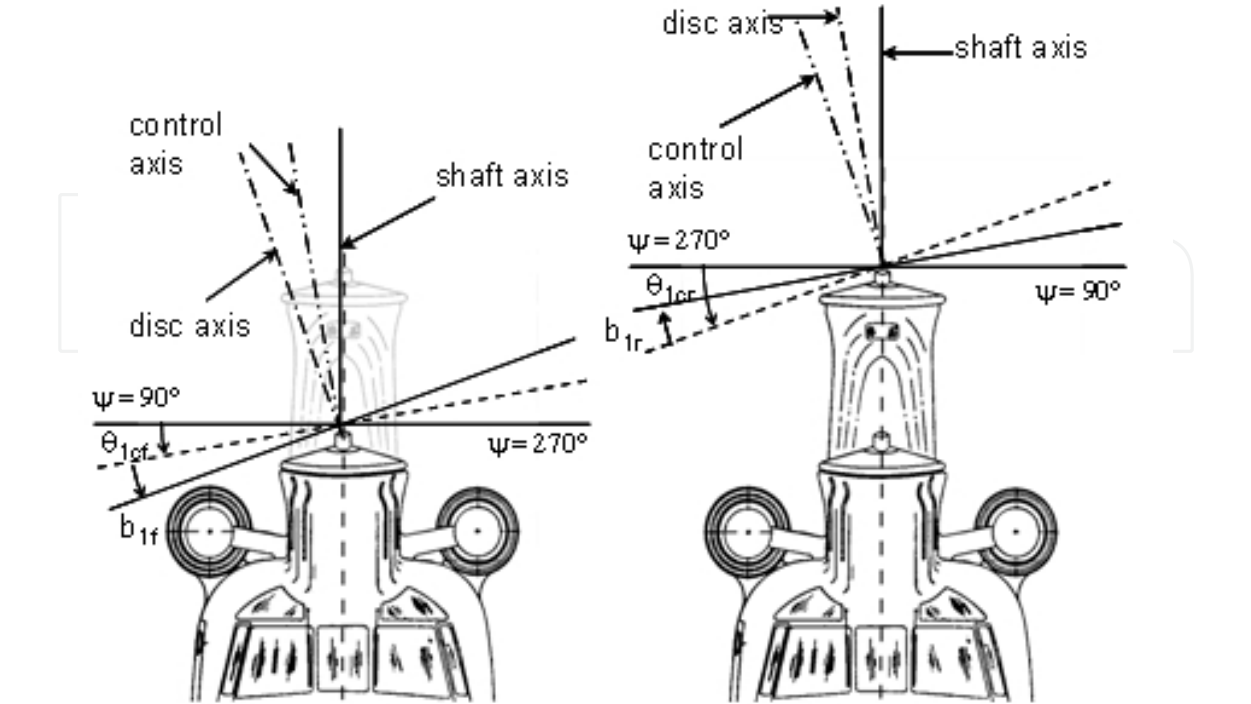


Fig. A4. Lateral axis Chinook control (front view)

The contributions of these components to the front rotor thrust and the horizontal and side forces in the helicopter body system are:

$$\begin{aligned}
 X_{Tf} &= T_f \sin(\theta_{1sf} - a_{1f} + i_f) \cos(\theta_{1cf} + b_{1f}) \\
 X_{Hf} &= -H_{xf} \cos(\theta_{1sf} - a_{1f} + i_f) - H_{yf} \sin(\theta_{1cf} + b_{1f}) \sin(\theta_{1sf} - a_{1f} + i_f) \\
 Y_{Tf} &= T_f \sin(\theta_{1cf} + b_{1f}) \cos(\theta_{1sf} - a_{1f} + i_f) \\
 Y_{Hf} &= H_{yf} \cos(\theta_{1cf} + b_{1f}) \\
 Z_{Tf} &= -T_f \cos(\theta_{1sf} - a_{1f} + i_f) \cos(\theta_{1cf} + b_{1f}) \\
 Z_{Hf} &= -H_{xf} \sin(\theta_{1sf} - a_{1f} + i_f) + H_{yf} \sin(\theta_{1cf} + b_{1f}) \sin(\theta_{1sf} - a_{1f} + i_f) \\
 L_{Qf} &= M_{Qf} \sin i_f \\
 N_{Qf} &= -M_{Qf} \cos i_f
 \end{aligned} \tag{9}$$

For the rear rotor, these components are (note the opposite direction of the lateral flapping angle b_{1r} with respect to the front rotor equations):

$$\begin{aligned}
 X_{Tr} &= T_r \sin(\theta_{1sr} - a_{1r} + i_r) \cos(\theta_{1cr} - b_{1r}) \\
 X_{Hr} &= -H_{xr} \cos(\theta_{1sr} - a_{1r} + i_r) + H_{yr} \sin(\theta_{1cr} - b_{1r}) \sin(\theta_{1sr} - a_{1r} + i_r) \\
 Y_{Tr} &= T_r \sin(\theta_{1cr} - b_{1r}) \cos(\theta_{1sr} - a_{1r} + i_r) \\
 Y_{Hr} &= -H_{yr} \cos(\theta_{1cr} - b_{1r}) \\
 Z_{Tr} &= -T_r \cos(\theta_{1sr} - a_{1r} + i_r) \cos(\theta_{1cr} - b_{1r}) \\
 Z_{Hr} &= -H_{xr} \sin(\theta_{1sr} - a_{1r} + i_r) - H_{yr} \sin(\theta_{1cr} - b_{1r}) \cos(\theta_{1sr} - a_{1r} + i_r) \\
 L_{Qr} &= -M_{Qr} \sin i_r \\
 N_{Qr} &= M_{Qr} \cos i_r
 \end{aligned} \tag{10}$$

The front and the rear rotor thrust (T_f and T_r), horizontal force (drag force) (H_{xf} , H_{xr}), lateral forces (H_{yf} , H_{yr}) and torque (M_{Qf} , M_{Qr}) are expressed by their non-dimensional coefficients:

$$\begin{aligned}
 T_{f,r} &= C_{Tf,r} \rho (\Omega R)^2 \pi R^2 \\
 H_{xf,r} &= C_{Hxf,r} \rho (\Omega R)^2 \pi R^2 \\
 H_{yf,r} &= C_{Hyf,r} \rho (\Omega R)^2 \pi R^2 \\
 M_{Qf,r} &= C_{Qf,r} \rho (\Omega R)^2 \pi R^3
 \end{aligned} \tag{11}$$

The non-dimensional coefficients for rotor thrust, horizontal and lateral forces and torque can be calculated using the blade element theory by integration of the lift and drag forces on each blade element along the blade and around the azimuth. Their non-dimensional coefficients w.r.t. the disc plane (non-dimensionalized by $\rho (\Omega R)^2 (\pi R^2)$), for the front and rear rotors, are:

$$C_{Tf,r} \approx C_{T,elem,f,r} = \frac{\sigma C_{la}}{2} \left[\frac{\theta_{0f,r}}{3} \left(1 + \frac{3}{2} \mu_{xf,r} \right) + \frac{\mu_{zf,r} - \lambda_{yf,r}}{2} \right] \quad (12)$$

$$C_{HXf,r} = \frac{\sigma C_{la}}{2} \left[\frac{\mu_{xf,r} C_{df,r}}{2 C_{la}} + \theta_{0f,r} \left(\frac{a_{1f,r}}{3} - \frac{\mu_{xf,r} \mu_{zf,r} - \lambda_{yf,r}}{2} \right) + \frac{3(\mu_{zf,r} - \lambda_{yf,r}) a_{1f,r}}{2} + \frac{\mu_{xf,r}}{4} (a_{0f,r}^2 + a_{1f,r}^2) - \frac{a_{0f,r} b_{1f,r}}{6} \right] - C_{Tf,r} a_{1f,r} \quad (13)$$

$$C_{HYf,r} = \frac{\sigma C_{la}}{2} \left[\mu_{xf,r}^2 \left(\frac{b_{1f,r} \theta_{0f,r}}{2} - a_{0f,r} a_{1f,r} \right) + \mu_{xf,r} \cdot \left(\frac{a_{1f,r} b_{1f,r}}{4} + \frac{3(\mu_{zf,r} - \lambda_{yf,r}) a_{0f,r}}{2} - \frac{3 a_{0f,r} \theta_{0f,r}}{4} \right) + \frac{\theta_{0f,r} b_{1f,r}}{3} + \frac{3(\mu_{zf,r} - \lambda_{yf,r}) b_{1f,r}}{4} + \frac{a_{0f,r} a_{1f,r}}{6} \right] - C_{Tf,r} b_{1f,r} \quad (14)$$

The main rotor thrust coefficient in Glauert theory is:

$$C_{T,Glau} = 2 \lambda_{yf,r} \sqrt{\mu_{xf,r}^2 + (\lambda_{yf,r} - \mu_{zf,r})^2} \quad (15)$$

The rotor torque coefficient can be expressed as:

$$C_{Qf,r} = \frac{\sigma C_{df,r}}{8} (1 + 4.7 \mu_{xf,r}^2) - C_{Tf,r} (\mu_{zf,r} - \lambda_{yf,r}) - \mu_{xf,r} C_{HXf,r} \quad (16)$$

The advance ratios of front/rear rotors $\mu_{xf,r}$, $\mu_{yf,r}$, $\mu_{zf,r}$ are calculated by projecting helicopter velocity vector (u,v,w) on the plane of front/rear rotor hub as $(u_{f,r}, v_{f,r}, w_{f,r})$:

$$\begin{bmatrix} u_f \\ v_f \\ w_f \end{bmatrix} = \begin{bmatrix} u + f_1 r - h_f q \\ v + l_f r + h_f p \\ w - l_f q - f_1 p \end{bmatrix} ; \quad \begin{bmatrix} u_r \\ v_r \\ w_r \end{bmatrix} = \begin{bmatrix} u + f_1 r - h_r q \\ v - l_r r + h_r p \\ w + l_r q - f_1 p \end{bmatrix} \quad (17)$$

and then by non-dimensionalizing $(u_{f,r}, v_{f,r}, w_{f,r})$ by ΩR while neglecting the yaw rate r . This leads to the following expressions for the front/rear rotor advance ratios:

$$\begin{aligned} \mu_{xf} &= \frac{(u - h_f q)}{\Omega R} & \mu_{yf} &= \frac{(v + h_f p)}{\Omega R} & \mu_{zf} &= \frac{(w - l_f q)}{\Omega R} \\ \mu_{xr} &= \frac{(u - h_r q)}{\Omega R} & \mu_{yr} &= \frac{(v + h_r p)}{\Omega R} & \mu_{zr} &= \frac{(w + l_r q)}{\Omega R} \end{aligned} \quad (18)$$

The blade drag coefficient $C_{df,r}$ of front/rear rotors is calculated as:

$$C_{df,r} = C_{d0} + C_{dt} C_{Tf,r}^2 \quad (19)$$

with the values C_{d0} and C_{dt} defined in Appendix B. The rotor interference is considered through interference factors expressed as in (Ostroff, Downing and Rood, 1976):

$$\begin{aligned} d\text{interf}_{f\text{-on-r}} &= \left[0.356 + 0.321\chi_{lf} - 0.368\chi_{lf}^2 + 0.392\chi_{lf}^3 \right] (1 - |\sin \beta_{fr}|) + \\ &\quad + \left[0.356 + 0.0131\chi_{lf} - 0.0764\chi_{lf}^2 - 0.0085\chi_{lf}^3 \right] \cdot |\sin \beta_{fr}| \\ d\text{interf}_{r\text{-on-f}} &= \left[0.356 + 0.151\chi_{lr} - 0.314\chi_{lr}^2 + 0.164\chi_{lr}^3 \right] (1 - |\sin \beta_{rr}|) + \\ &\quad + \left[0.356 + 0.0131\chi_{lr} - 0.0764\chi_{lr}^2 - 0.0085\chi_{lr}^3 \right] \cdot |\sin \beta_{rr}| \end{aligned} \quad (20)$$

where χ_{lf} , χ_{lr} are the inflow angles of front and rear rotors defined as in Figure A5 and equation (21) and β_{fr} and β_{rr} are rotor sideslip angles defined in equation (22) and (17).

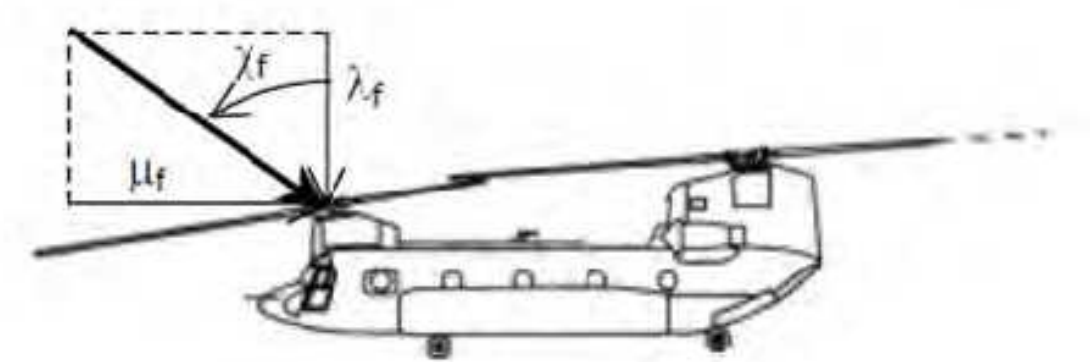


Fig. A5. Rotor inflow angle used to calculate front and rear rotor interferences

$$\chi_{lf} = \arctan \left(\frac{\mu_{xf}}{\lambda_f} \right) \quad \chi_{lr} = \arctan \left(\frac{\mu_{xr}}{\lambda_r} \right) \quad (21)$$

$$\begin{aligned} \sin \beta_{fr} &= v_f / \sqrt{u_f^2 + v_f^2} & \cos \beta_{fr} &= u_f / \sqrt{u_f^2 + v_f^2} & u_f &\neq 0 \\ \sin \beta_{rr} &= v_r / \sqrt{u_r^2 + v_r^2} & \cos \beta_{rr} &= u_r / \sqrt{u_r^2 + v_r^2} & u_r &\neq 0 \end{aligned} \quad (22)$$

The interference factors are used to compute a new inflow ratio in the Glauert formula (15):

$$\begin{aligned} \lambda_{f,\text{new}} &= \frac{C_{Tf}}{2\sqrt{(\mu_{zf} - \lambda_{if})^2 + \mu_{xf}^2}} + d\text{interf}_{r\text{-on-f}} \frac{C_{Tr}}{2\sqrt{(\mu_{zr} - \lambda_{ir})^2 + \mu_{xr}^2}} \\ \lambda_{r,\text{new}} &= \frac{C_{Tr}}{2\sqrt{(\mu_{zr} - \lambda_{ir})^2 + \mu_{xr}^2}} + d\text{interf}_{f\text{-on-r}} \frac{C_{Tf}}{2\sqrt{(\mu_{zf} - \lambda_{if})^2 + \mu_{xf}^2}} \end{aligned} \quad (23)$$

The fuselage forces and moments are calculated through flat plate theory using (Ostroff, Downing and Rood, 1976):

$$\begin{aligned}
X_B &= -C_{FE} \frac{1}{2} \rho V^2 \cos \alpha_{fus} \cos \beta_{fus} \\
Y_B &= -C_{Y\beta} \frac{1}{2} \rho V^2 \sin \beta_{fus} \\
Z_B &= -C_{L\alpha} \frac{1}{2} \rho V^2 \sin \alpha_{fus} \\
L_B &= -C_{L\beta} \frac{1}{2} \rho V^2 \sin \beta_{fus} |\cos \beta_{fus}| (1 - |\sin \alpha_{fus}|) \\
M_B &= C_{M\alpha} \frac{1}{2} \rho V^2 \sin \alpha_{fus} \cos \alpha_{fus} \\
N_B &= -C_{N\beta} \frac{1}{2} \rho V^2 \sin \beta_{fus} \cos \beta_{fus} (0.94 \sin \alpha_{fus} + 0.342 \cos \alpha_{fus})
\end{aligned} \tag{24}$$

where the fuselage angle of attack α_{fus} and fuselage sideslip β_{fus} are defined as seen as:

$$\begin{aligned}
\sin \alpha_{fus} &= w / \sqrt{u^2 + w^2} & \cos \alpha_{fus} &= u / \sqrt{u^2 + w^2} \\
\sin \beta_{fus} &= v / \sqrt{u^2 + v^2} & \cos \beta_{fus} &= u / \sqrt{u^2 + v^2}
\end{aligned} \tag{25}$$

The helicopter has three suspension points $i=1,2,3$ underneath its floor as seen in Fig. A6, the tension force in one cable j being S_{ij} . The total forces on the slings are:

$$\begin{aligned}
X_S &= S_{ij} \cos \alpha_{ij} \sin \beta_{ij} \\
Y_S &= S_{ij} \sin \alpha_{ij} \sin \beta_{ij} \\
Z_S &= S_{ij} \cos \beta_{ij} \\
L_S &= -S_{ij} \{ \sin \alpha_{ij} \sin \beta_{ij} h_{s_i} - \cos \beta_{ij} f_1 \} \\
M_S &= S_{ij} \cos \alpha_{ij} \sin \beta_{ij} h_{s_i} - S_{1,3j} \cos \beta_{1,3j} f_{s_{1,3}} + S_{2j} \cos \beta_{2j} f_{s_2} \\
N_S &= S_{ij} \cos \alpha_{ij} \sin \beta_{ij} f_1 + S_{1,3j} \sin \alpha_{1,3j} \sin \beta_{1,3j} f_{s_{1,3}} - S_{2j} \sin \alpha_{2j} \sin \beta_{2j} f_{s_2}
\end{aligned} \tag{26}$$

where α_{ij} and β_{ij} are the angles that the sling cable makes with the X and Z direction; $f_{s_{1,2,3}}$ and $h_{s_{1,2,3}}$ are the hook distances to the helicopter centre of gravity. The slings are modelled as linear springs without mass and have small internal damping. The tension force in each cable is determined by comparing the actual sling length l_{ij} to the zero tension sling length l_{0ij} , see equation (27), where j is the cable number on the i^{th} suspension point. The zero tension cable length as well as the cable stiffness are known, the actual length of each cable is computed by measuring the distance between the specific helicopter suspension point and the suspension point on the load.

$$S_{ij} = \max \{ 0, k(l_{ij} - l_{0ij}) \} \tag{27}$$

The damping forces inside the slings are determined using equation (28). In this equation dV is the relative velocity between the endpoints of a cable, in the direction of that cable. This requires that both endpoint velocities are known in the same axis system. The damping coefficient is set just large enough to prevent the load from increase in pendulum motion when the load is oscillating around a fixed point.

$$S_{damp,ij} = dV_{ij} c_{damp} \tag{28}$$

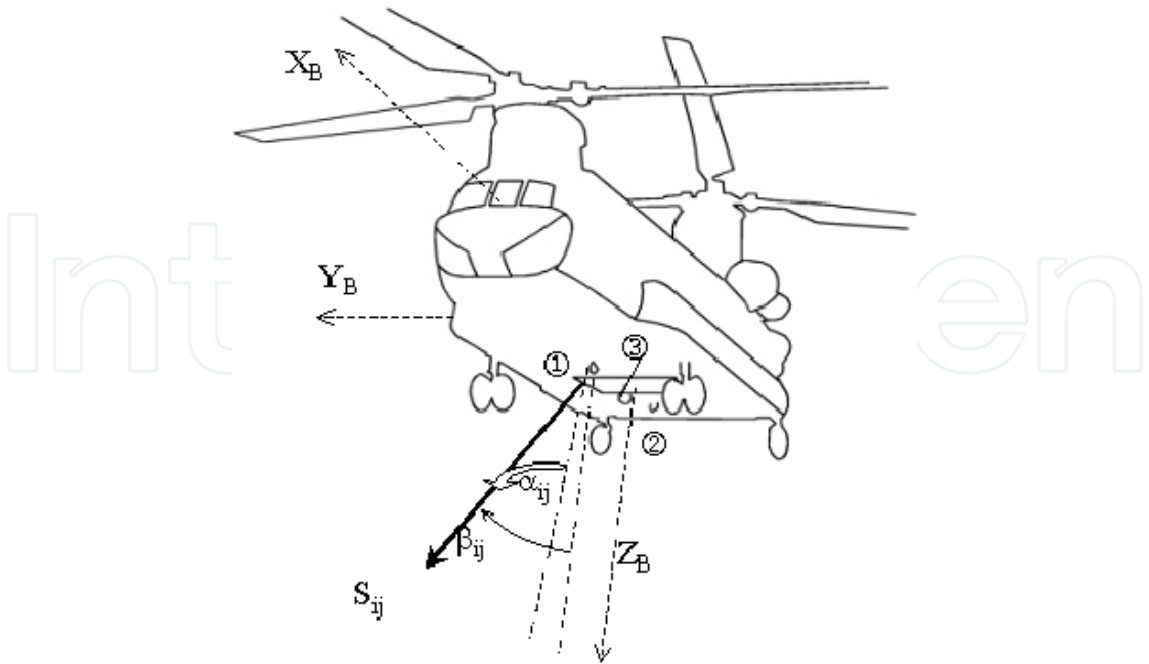


Fig. A6. Hooks and slings loads

7.2 Load model

The load is modelled as a 6-dof body, the helicopter slings being connected to the load as seen in Fig. A7.

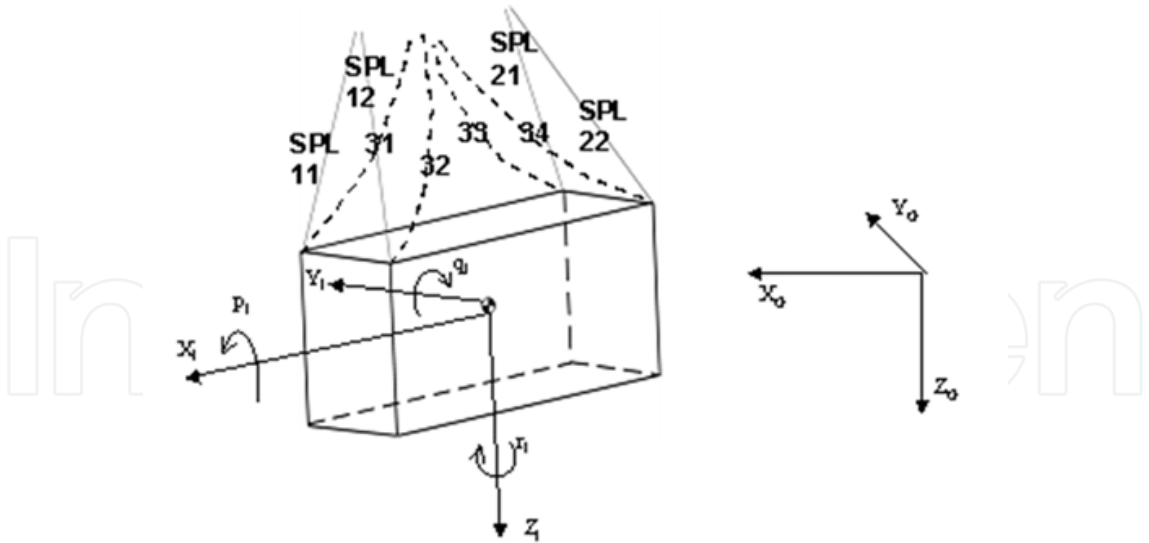


Fig. A7. Container load with local axes and sling numbering

The forces and moments acting on the load centre of gravity, besides load gravitational forces, consist of cable forces indexed with C and aerodynamic forces, which are determined using flat plate theory, indexed Bl . The summation of these forces and moments is given by equation (29).

$$\begin{aligned} X_l &= X_c + X_{Bl} \\ Y_l &= Y_c + Y_{Bl} \\ Z_l &= Z_c + Z_{Bl} \\ L_l &= L_c + L_{Bl} \\ M_l &= M_c + M_{Bl} \\ N_l &= N_c + N_{Bl} \end{aligned}$$

(29)

The contributions of each cable and of the load aerodynamics are given in equations (30) and (31) respectively. Note that the cable component is valid only for a V-suspension.

$$\begin{aligned} X_c &= S_{ij} \cos \alpha_{lij} \sin \beta_{lij} \\ Y_c &= S_{ij} \sin \alpha_{lij} \sin \beta_{li1} \\ Z_c &= -S_{ij} \cos \beta_{lij} \\ L_c &= S_{ij} \sin \alpha_{lij} \sin \beta_{lij} h_{cgl} - S_{i1} \cos \beta_{li1} w_{cgl} + S_{i2} \cos \beta_{li2} (w_l - w_{cgl}) \\ M_c &= -S_{ij} \cos \alpha_{lij} \sin \beta_{lij} h_{cgl} + S_{1j} \cos \beta_{li1} l_{cgl} - S_{2j} \cos \beta_{li2} (l_l - l_{cgl}) \\ N_c &= +S_{1j} \sin \alpha_{li1} \sin \beta_{li1} l_{cgl} - S_{2j} \cos \alpha_{li2} \sin \beta_{li2} (l_l - l_{cgl}) \\ &\quad - S_{i1} \cos \alpha_{li1} \sin \beta_{li1} w_{cgl} + S_{i2} \cos \alpha_{li2} \sin \beta_{li2} (w_l - w_{cgl}) \end{aligned}$$

(30)

The magnitude of the sling forces is given by equation (27). The load aerodynamics are taken from the flat plate theory, using the empirical equations of reference (Ostroff, Downing and Rood, 1976), see equation (31).

$$\begin{aligned} X_{Bl} &= -C_{FEI} \frac{1}{2} \rho V_l^2 \\ Y_{Bl} &= -C_{Y\beta l} \frac{1}{2} \rho V_l^2 \sin \beta_{sl} \\ Z_{Bl} &= -C_{L\alpha l} \frac{1}{2} \rho V_l^2 \sin \alpha_{sl} \\ L_{Bl} &= -C_{L\beta l} \frac{1}{2} \rho V_l^2 \sin \beta_{sl} |\cos \beta_{sl}| (1 - |\sin \alpha_{sl}|) \\ M_{Bl} &= C_{M\alpha} \frac{1}{2} \rho V_l^2 \sin \alpha_{sl} \cos \alpha_{sl} \\ N_{Bl} &= -C_{N\beta} \frac{1}{2} \rho V_l^2 \sin \beta_{sl} \cos \beta_{sl} (0.94 \sin \alpha_{sl} + 0.342 \cos \alpha_{sl}) \end{aligned}$$

(31)

8. Appendix B

Data for the helicopter and load used in the simulation model

Chinook dimensions (see Fig. B1)	
h _f	2.093 m
h _r	3.527 m
l _f	6.425 m
l _r	5.450 m
f ₁	0 m
fs ₁	2.28092 m
fs ₂	1.78308 m
fs ₃	0.19812 m
hs _{1,2}	1.309 m
hs ₃	1.509 m

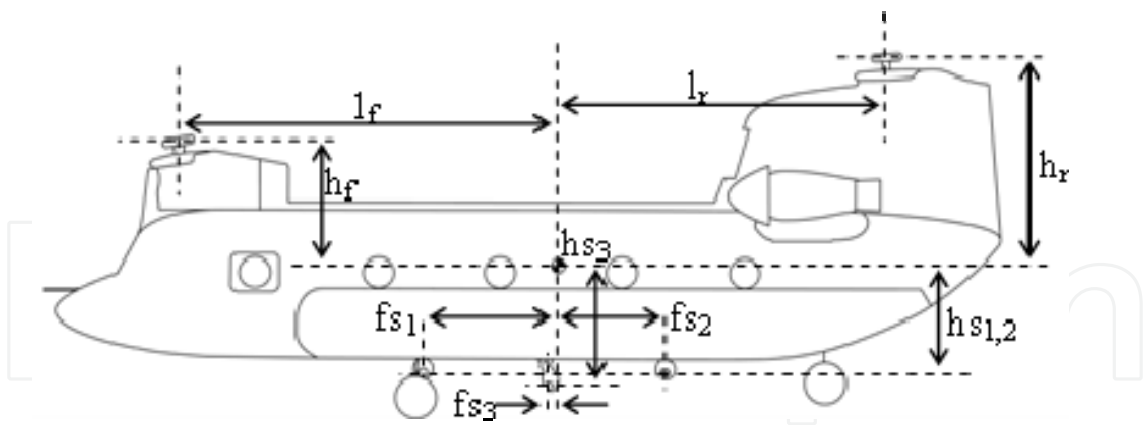


Fig. B1. Chinook dimensions

Rotor characteristics	
m_{bl}	161 kg
σ	0.08459
N	3
i_f	9 deg
i_r	4 deg
Ω	23.562 rad/s
γ	12.8
θ_{twist}	- 9.14 deg
R	9.144 m
c	0.81m
$C_{l\alpha}$	5.75 rad ⁻¹
C_{do}	0.0098
C_{dt}	38.66

Chinook mass and moments of inertia	
m	14968.6 kg
I_x	50386.3 kg m ²
I_y	273536 kg m ²
I_z	257685 kg m ²
I_{xz}	19838.3 kg m ²
I_{bl}	3110.2 kg m ²

Chinook CH-47B aerodynamics	
C_{FE}	3.5 m ²
$C_{L\alpha fus}$	32.5 m ²
$C_{L\beta}$	6.57 m ³
$C_{M\alpha}$	142 m ³
$C_{N\beta}$	51.5 m ³
$C_{Y\beta}$	43.4 m ²

Blade control angle to stick displacement conversion factors	
Collective front rotor	0.734 deg/cm
Collective rear rotor	0.734 deg/cm
Longitudinal front rotor	0.242 deg/cm
Longitudinal rear rotor	-0.242 deg/cm
Lateral front rotor	0.752 deg/cm
Lateral rear rotor	-0.752 deg/cm
Pedal front rotor	1.25 deg/cm
Pedal rear rotor	- 1.25 deg/cm
Collective front/rear neutral	7.85 deg

Blade control system limits	deg	cm stick
Collective range front rotor	0 – 16 deg	0 – 21.8 cm
Collective range rear rotor	0 – 16 deg	
Longitudinal cyclic range front rotor	- 0.5 – 2 deg	-2 – 10.33 cm
Longitudinal cyclic range rear rotor	- 0.5 – 2.5 deg	
Lateral cyclic angle front rotor	- 10 – 10 deg	-13 – 13 cm
Lateral cyclic angle rear rotor	- 10 – 10 deg	

Container load mass and dimensions	
m_l	2000, 6000 and 10000 kg
l_l	6.058 m
w_l	2.438 m
h_l	2.591 m
$l_{CG\ l}$	$(\frac{1}{2} l_l)$ m
$w_{CG\ l}$	$(\frac{1}{2} w_l)$ m
$h_{CG\ l}$	$(\frac{1}{2} h_l)$ m

Load moments of inertia	
$I_{xx\ l}$	$\frac{1}{12} m_l (w_l^2 + h_l^2)$
$I_{yy\ l}$	$\frac{1}{12} m_l (h_l^2 + l_l^2)$
$I_{zz\ l}$	$\frac{1}{12} m_l (w_l^2 + l_l^2)$
$I_{xz\ l}$	0

Load moments of inertia	
I_{xx1}	$\frac{1}{12}m_l(w_l^2 + h_l^2)$
I_{yy1}	$\frac{1}{12}m_l(h_l^2 + l_l^2)$
I_{zz1}	$\frac{1}{12}m_l(w_l^2 + l_l^2)$
I_{xz1}	0

Sling aerodynamics	
k	$7.25 \cdot 10^5 \text{ N/m}$
k_{red}	$1 \cdot 10^5 \text{ m}^2/\text{rad}$
$I_{normal\ ij}$	4 m
I_{red}	5.2 m
c_{damp}	10 kg/s

9. Acknowledgment

The subject of this research was initiated as collaboration between Delft University of Technology, TNO Defence, Security and Safety and Royal Netherlands Air Force (RNLAf). Sincere thanks for all support given by the Chinook pilots to judge the results.

10. References

ADS-33 (2000) *Aeronautical Design Standard-33E-PRE, Performance Specification, Handling Qualities Requirements for Military Rotorcraft*, US Army AMCOM, Redstone, Alabama

Anon. (2002) *Technical Manual, Aviation Unit and Aviation Intermediate Maintenance Manual CH-47D Helicopter*, TM 55-1520-240-23-9, Headquarters, Department of the Army, Rev. 19 Sept. 2002, chapter 11, section IX, page 1012

Anon, (2004), *Boeing Integrated Defense Systems, ICH-47D-10: Flight Manual International CH-47D Helicopter*, The Boeing Company, 2004

Bisgaard, Morten, Bendtsen, Jan Dimon, la Cour-Habo, Anders (2006) *Modelling of Generic Sling Load System*, AIAA Modeling and Simulation Technologies Conference and Exhibit, 21-24 Aug. 2006, Keystone, Colorado, AIAA 2006-6816

Boeing Helicopters (2004), *Flight Manual International CH-47D Helicopter*, The Boeing Company, Philadelphia, Pennsylvania, Rev 4, 30 September 2004.

Chen, C., Lim, K.Y. and Seah, C.S.P.(1998) *Modeling and Dynamic Analysis of Helicopter Underslung System*”, *AIAA Modeling and Simulation Technologies Conference and Exhibit*, 10-12 Aug. 1998, Boston, MA, AIAA-98-4358

Cicolani, Luigi S., Kanning, Gerd, Synnestvedt, Robert (1995) *Simulation of the Dynamics of Helicopter Slung Load Systems. J. of the American Helicopter Society*, Vol. 40, No. 4, October 1995, pp. 44-61

Cliff, E.M. and Bailey (1975) D.B., *Dynamic Stability of a Translating Vehicle with a Simple Sling Load*, *J. of Aircraft*, Vol. 12, No. 10, Oct. 1975

- Dukes, Theodor, A. (1973) Maneuvring Heavy Sling Loads Near Hover Part II: Some Elementary Maneuvres, *J. of the American Helicopter Society*, Vol. 18, No. 3, July 1973, pp. 3-13
- Dukes, Theodor, A. (1973) Maneuvring Heavy Sling Loads Near Hover Part II: Some Elementary Maneuvres, *J. of the American Helicopter Society*, Vol. 18, No. 3, July 1973, pp. 3-13
- Eindhoven P., et al. (2006) Development of Control Laws for the Chinook Digital AFCS program, *62nd American Helicopter Society Annual Forum*, May 9-11, 2006, Phoenix, Arizona
- Fusato, Dario, Guglieri, Giorgio, Celi, Roberto (2001) Flight Dynamics of an Articulated Rotor Helicopter with an External Load, *J. of the American Helicopter Society*, Vol. 46, No. 1, January 2001, pp. 3-12
- Gabel, Richard, Wilson, Gregory, J. (1968). Test Approaches to External Sling Load Instabilities, *J. of American Helicopter Society*, Vol. 13, No.3, July 1968, pp. 44-54
- Kendrick, Stephen, A., Walker, Daniel, J. (2006) The Modelling, Simulation and Control of Helicopters Operating with External Loads, *62nd Annual Forum of the American Helicopter Society*, May 9-11, 2006, Phoenix, AZ
- Lucassen, L.R., and Stenk F.J.(1965) Dynamic Stability Analysis of a Hovering Helicopter with a Slung Load", *J. of the American Helicopter Society*, 10(2), pp.. 1965
- Nagabhushan, B.L. (1985). Low-Speed Stability Characteristics of a Helicopter with a Sling Load", *VERTICA*, Vol. 9, No.4, 1985, pp. 345-361
- Ostroff A.J., Downing, D.R. And Rood, W.J. (1976) A technique using a non-linear helicopter model for determining trims and derivatives, NASA TN D-8159, Langley Research Center Hampton, Va, May 1976
- Pavel, M.D.(2007) Mathematical Modeling of Tandem Helicopters with External Sling Loads for Piloted Simulation, AIAA Modeling and Simulation Technologies Conference and Exhibit, Hilton Head, South Carolina, IAA-2007-6617
- Pavel, M.D. (2010) Investigation of Chinook helicopter operations with an external slung load after cable failure. *The Aeronautical Journal*, 114(1156), pp. 345-365
- Feaster, L., Poli, C. & Kirchhoff, R. (1977) Dynamics of a Slung Load, *J. of Aircraft*, Vol. 14, No. 2, pp. 115-121
- Prabhakar, A. (1978) Stability of a Helicopter Carrying an Underslung Load, *VERTICA*, Vol.2, No.2, 1978, pp. 121-143
- Prouty, R.W. (2001) *Longitudinal cyclic control for tandem-rotor helicopters*, VERTIFLITE magazine, vol. 47, no. 3. 2001
- Reijm, Rogier, Pavel, Marilena D&, Bart, Jacob (2006), Effects of Automatic Flight Control System on Chinook Underslung Failures, *32nd European Rotorcraft Forum*, Maastricht, The Netherlands, September, 12-14, 2006
- Sheldon, D.F. (1977) An Appreciation of the Dynamic Problems Associated with the External Transportation of Loads from a Helicopter-State of the Art, *VERTICA*, Vol. 1, 1977
- Stuckey, R.A. (2002) *Mathematical Modelling of helicopter Slung-load systems*, DSTO Aeronautical and Maritime Research Laboratory, Victoria Australia, 2002
- Tyson, Peter, et. al. (1999). Simulation Prediction and Flight Validation of UH-60A Black Hawk Slung load Characteristics, *55th American Helicopter Society Annual Forum*, May 25-27, 1999, Montreal, Canada

Van der Kamp, Reinier., et. al. (2005). Investigation on the Chinook operations with an external sling load after cable failure”, *31st European Rotorcraft Annual Forum*, Florence, Italy, September 13-15, 2005

IntechOpen

IntechOpen



Automatic Flight Control Systems - Latest Developments

Edited by Dr. Thomas Lombaerts

ISBN 978-953-307-816-8

Hard cover, 204 pages

Publisher InTech

Published online 18, January, 2012

Published in print edition January, 2012

The history of flight control is inseparably linked to the history of aviation itself. Since the early days, the concept of automatic flight control systems has evolved from mechanical control systems to highly advanced automatic fly-by-wire flight control systems which can be found nowadays in military jets and civil airliners. Even today, many research efforts are made for the further development of these flight control systems in various aspects. Recent new developments in this field focus on a wealth of different aspects. This book focuses on a selection of key research areas, such as inertial navigation, control of unmanned aircraft and helicopters, trajectory control of an unmanned space re-entry vehicle, aeroservoelastic control, adaptive flight control, and fault tolerant flight control. This book consists of two major sections. The first section focuses on a literature review and some recent theoretical developments in flight control systems. The second section discusses some concepts of adaptive and fault-tolerant flight control systems. Each technique discussed in this book is illustrated by a relevant example.

How to reference

In order to correctly reference this scholarly work, feel free to copy and paste the following:

Marilena D. Pavel (2012). Effects of Automatic Flight Control System on Chinook Underslung Load Failures, Automatic Flight Control Systems - Latest Developments, Dr. Thomas Lombaerts (Ed.), ISBN: 978-953-307-816-8, InTech, Available from: <http://www.intechopen.com/books/automatic-flight-control-systems-latest-developments/effects-of-automatic-flight-control-system-on-chinook-underslung-load-failures>

INTECH
open science | open minds

InTech Europe

University Campus STeP Ri
Slavka Krautzeka 83/A
51000 Rijeka, Croatia
Phone: +385 (51) 770 447
Fax: +385 (51) 686 166
www.intechopen.com

InTech China

Unit 405, Office Block, Hotel Equatorial Shanghai
No.65, Yan An Road (West), Shanghai, 200040, China
中国上海市延安西路65号上海国际贵都大饭店办公楼405单元
Phone: +86-21-62489820
Fax: +86-21-62489821

© 2012 The Author(s). Licensee IntechOpen. This is an open access article distributed under the terms of the [Creative Commons Attribution 3.0 License](https://creativecommons.org/licenses/by/3.0/), which permits unrestricted use, distribution, and reproduction in any medium, provided the original work is properly cited.

IntechOpen

IntechOpen